BIOCHEMISTRY
including biophysical chemistry & molecular biology

Article

pubs.acs.org/biochemistry

Replication-Competent Influenza Virus and Respiratory Syncytial Virus Luciferase Reporter Strains Engineered for Co-Infections Identify Antiviral Compounds in Combination Screens

Dan Yan,[†] Marco Weisshaar,[†] Kristen Lamb,[†] Hokyung K. Chung,[‡] Michael Z. Lin,[§,∥] and Richard K. Plemper*[,†]

[†]Institute for Biomedical Sciences, Georgia State University, Atlanta, Georgia 30303-3222, United States
[‡]Department of Biology, Stanford University, Stanford, California 94305-5020, United States
[§]Department of Bioengineering, Stanford University, Stanford, California 94305, United States
[∥]Department of Pediatrics, Stanford University, Stanford, California 94305, United States

Supporting Information

ABSTRACT: Myxoviruses such as influenza A virus (IAV) and respiratory syncytial virus (RSV) are major human pathogens, mandating the development of novel therapeutics. To establish a high-throughput screening protocol for the simultaneous identification of pathogen- and host-targeted hit candidates against either pathogen or both, we have attempted co-infection of cells with IAV and RSV. However, viral replication kinetics were incompatible, RSV signal window was low, and an IAV-driven minireplicon reporter assay used in initial screens narrowed the host cell range and restricted the assay to single-cycle infections. To overcome these limitations, we developed an RSV strain carrying firefly luciferase fused to an innovative universal small-molecule assisted shut-off domain, which boosted assay signal window, and a hyperactive fusion protein that synchronized IAV and RSV reporter expression kinetics and suppressed the identification of RSV entry inhibitors sensitive to a recently reported RSV pan-resistance mechanism. Combined with a replication-competent recombinant IAV strain harboring nanoluciferase, the assay performed well on a human respiratory cell line and supports multicycle infections. Miniaturized to 384-well format, the protocol was validated through screening of a set of the National Institutes of Health Clinical Collection (NCC) in quadruplicate. These test screens demonstrated favorable assay parameters and reproducibility. Application to a LOPAC library of bioactive compounds in a proof-of-concept campaign detected licensed antimyxovirus therapeutics, ribavirin and the neuraminidase inhibitor zanamivir, and identified two unexpected RSV-specific hit candidates, Fenretinide and the opioid receptor antagonist BNTX-7. Hits were evaluated in direct and orthogonal dose−response counterscreens using a standard recRSV reporter strain expressing Renilla luciferase.

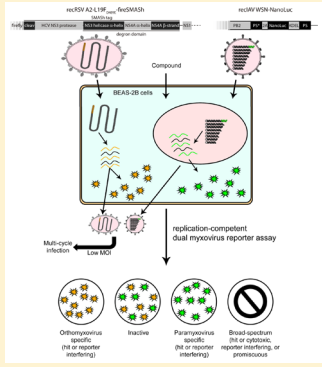

The myxovirus families include major human respiratory pathogens such as influenza virus, RSV, measles virus (MeV), and the highly pathogenic henipaviruses.[1] Of these, RSV and the influenza viruses are pharmaceutically most relevant.

RSV, a member of the paramyxovirus family, is the leading cause of infant hospitalization due to viral infection in the United States and responsible for the majority of viral deaths among children <1 year of age.[2] Approximately 1% of the winter infant cohort (~125000 patients) is hospitalized in the United States with RSV disease annually.[2,3] Infants born prematurely or born with bronchopulmonary dysplasia or a congenital heart defect are at highest risk of developing severe RSV disease.[4] While re-infection with RSV can occur throughout life,[5] RSV is life-threatening to the elderly and the immunocompromised.[6]

Clinical symptoms of human infection by major paramyxovirus pathogens such as MeV are dominated by host immunopathology,[7] closing the window for therapeutic intervention after the onset of symptoms.[8] In the case of RSV, however, several studies have challenged the paradigm that RSV pathogenesis is the result of host immunopathology alone. Higher viral loads were identified as a prediction of severe lower-respiratory RSV infection in infants,[9] and RSV load on day 3 after hospitalization was associated with a requirement for intensive care and respiratory failure in children <2 years of age.[10] These observations suggest that efficacious therapeutics given early to hospitalized children may improve downstream morbidity and reduce immunopathology, opening an opportunity for improved disease management. While RSV elicits innate and adaptive immune responses, the virus is poorly immunogenic overall and neutralizing antibody titers wane quickly postinfection,[5] making vaccine development

Received: June 5, 2015
Revised: August 4, 2015
Published: August 26, 2015

DOI: 10.1021/acs.biochem.5b00623
Biochemistry 2015, 54, 5589−5604

challenging despite extensive research. Immunoprophylaxis with the neutralizing antibody palivizumab is reserved for high-risk patients because of prohibitive costs,[11] and ribavirin, although approved for RSV treatment, has little clinical benefit due to efficacy and toxicity issues.[12]

IAV accounts for 3−5 million infections per year, representing the overall leading cause of human respiratory disease due to viral infection.[13] In the United States alone, seasonal influenza alone is responsible for 20000−40000 deaths per year and poses a substantial economic burden due to decreased productivity and healthcare costs associated with hospitalization and/or treatment.[13] Morbidity and mortality associated with pandemic and emerging, highly pathogenic influenza strains can be substantially higher.[14−16]

The current seasonal influenza vaccines show efficacy in 70% of vaccinated adults but only 40% of the elderly.[1,17−19] Neuraminidase inhibitors make up the predominant class of anti-influenza virus therapeutics, and oseltamivir is still the primary drug stockpiled for pandemic preparedness. It is recommended for treatment of seasonal IAV H1N1, H3N2, and influenza B virus strains.[20] However, efficacy in humans is moderate[21] and is a subject of debate.[22−24] The issue is aggravated by the emergence of resistance to oseltamivir, which affects seasonal, pandemic, and highly pathogenic avian influenza strains.[18,19]

The development of a novel therapeutic against IAV and RSV infections is urgently needed to address the significant morbidity and mortality, the high socioeconomic toll, and the emergence of strains with preexisting resistance against available antivirals that we experience with these pathogens.[25,26] Host-targeted antivirals have experienced a renaissance in the past decade based on the promise of combining low frequencies of emerging viral resistance with a broadened antiviral indication spectrum.[27−29] However, the host-directed approach is inherently at a higher risk of inducing unacceptable side effects, and efficacy can be compromised by alternative host pathways that my functionally replace the therapeutically targeted pathway *in vivo*.[30,31]

While there are tangible advantages associated with host-directed antivirals, narrowly designed drug discovery campaigns are inherently challenged by the risk of early stage failure due to a shallow candidate pool. In search of a resource-effective approach that simultaneously interrogates the full host−pathogen interactome for both pathogen-directed and host-directed hit candidates in a single-well setting, we have recently described a dual myxovirus pathogen high-throughput screening (HTS) assay.[32] On the basis of the hypothesis that the anticipated broadened indication spectrum of host-directed antivirals itself can be employed as the selector for hit candidates, we combined in this first implementation of the strategy an IAV isolate driving a firefly luciferase minigenome reporter with a recombinant MeV reporter strain expressing Renilla luciferase. MeV, a paramyxovirus, was chosen as a replacement for RSV, because we found that fast IAV and slow RSV reporter expression kinetics were incompatible.[32] We demonstrated that ortho- and paramyxoviruses efficiently coreplicate, thus allowing the automated identification of orthomyxovirus-specific, paramyxovirus-specific, and broad-spectrum drug candidates in a robust assay format. Implementation of this dual-pathogen protocol in a proof-of-concept screen identified, among others, the pan-myxovirus blocker compound 09167, which acts by stimulating the expression of effector genes of host antiviral pathways.[32]

Despite this confirmation of general feasibility, the pilot screen also highlighted several limitations of the original assay. (i) The IAV minireplicon reporter is resource-intensive, because it mandates reporter plasmid transfection and cryopreservation of transfected cells prior to seeding into high-density assay plates. (ii) Expression of the minireplicon construct must be driven either by the T7 polymerase or by RNA polymerase I, which restricts the conceivable host cell range to cell lines stably expressing T7 polymerase or lines with high intrinsic RNA Pol I activity, such as 293T cells.[32] (iii) Poorly synchronized IAV and RSV reporter expression kinetics necessitated the use of a recombinant MeV reporter strain as a paramyxovirus surrogate, which excluded the identification of pathogen-directed RSV inhibitors. It was therefore the goal of this study to develop and implement in a feasibility screen innovative myxovirus reporter strains that overcome these limitations and support direct drug screens with replication-competent IAV and RSV reporter strains in a robust HTS campaign.

MATERIALS AND METHODS

Cell Lines and Transfections. Human carcinoma (HEp-2, ATCC CCL-23), human lung carcinoma (A549, ATCC CCL-185), human bronchial epithelial (BEAS-2B, ATCC CRL-9609), human embryonic kidney (293T, ATCC CRL-3216), and Madin Darby canine kidney (MDCK, ATCC CCL-34) cells were maintained at 37 °C and 5% CO_2 in Dulbecco's modified Eagle's medium (DMEM) supplemented with 7.5% fetal bovine serum. Baby hamster kidney (BHK-21) cells stably expressing T7 polymerase (BSR-T7/5 cells)[33] were incubated at every third passage in the presence of 500 μg/mL G-418 (Geneticin). Lipofectamine 2000 (Invitrogen) was used for all transient transfection reactions.

Generation of recIAV Reporter Strains. Recombinant IAV/WSN/33 (H1N1) (IAV-WSN) strains were generated using the eight-plasmid IAV rescue system.[34] Plasmids pHW12-PB1, pHW12-PB2, pHW12-PA, pHW12-NP, pHW12-HA, pHW12-NA, pHW12-M, and pHW12-NS were kind gifts from D. Steinhauer (Emory University, Atlanta, GA). Recombinant IAV-containing Renilla and Gaussia luciferase reporters in the NS1 and PB2 segments were generated as previously described.[35,36] recIAV-WSN harboring nanoluciferase in the PB2 segment was constructed like recIAV-WSN Gaussia. Briefly, the PB2 3′ packaging signal was inactivated through silent mutagenesis and a nanoluciferase-encoding open reading frame (ORF) harboring a 3′ KDEL-encoding endoplasmic reticulum retention signal fused to the mutant PB2 ORF through recombineering polymerase chain reaction (PCR). Nanoluciferase and Gaussia luciferase genes were amplified from plasmids pNL1.1CMV[Nluc/CMV] (Promega) and pTK-Gaussia (ThermoFisher), respectively. A 2A cleavage sequence from porcine teschovirus[37] was inserted between the PB2 and luciferase ORFs, and a copy of the original PB2 packaging signal was inserted downstream of the coding cassette. The sequences of all plasmids were confirmed.

IAV Recovery, Amplification, and Stability Testing. All recIAV strains were recovered through rescue plasmid transfection into 293T cells and overlay of transfected cells onto MDCK cells after incubation for 28 h. Recovered recombinants were amplified and released virions titered through a plaque assay on MDCK cells. For genetic stability testing, recombinant virions were passaged consecutively four times and virus titers determined through plaque assays after

DOI: 10.1021/acs.biochem.5b00623
Biochemistry 2015, 54, 5589−5604

each passage. In parallel, reporter titers were determined after each passage through 50% tissue culture infective dose ($TCID_{50}$) titration with bioluminescence as the readout, using a Synergy H1 (BioTek) multimode microplate reader equipped with substrate injectors.

Generation of recRSV Reporter Strains. The backbone for all recombinant RSV strains was a plasmid containing a full length cDNA copy of a chimeric RSV-A2 genome, in which the F-encoding open reading frame was replaced with that of the line19 (L19) RSV isolate and an additional Renilla luciferase ORF was added.[38] The D489E substitution was introduced into L19F through directed mutagenesis of a helper vector harboring a SacII/SalI fragment of the genome, followed by transfer into the full length plasmid and sequence confirmation, creating recRSV A2-L19F$_{D489E}$-renilla. Recombineering PCR was employed to add RSV intergenic junctions and flanking regions to firefly luciferase ORF, followed by substitution of a Renilla luciferase-containing BstBI/AvrII fragment in recRSV A2-L19F$_{D489E}$-renilla with the equivalent fragment harboring firefly luciferase. To generate the fireSMASh ORF, the SMASh tag[39] was fused in frame to the 3′ end of the firefly luciferase ORF through recombineering PCR, followed by addition of the RSV flanking regions and BstBI/AvrII transfer into the full length cDNA genome copy as before. recRSV were recovered through cotransfection with RSV L, N, P, and M2-encoding helper plasmids into BSR-T7/5 cells as previously described[38] and subjected to RT-PCR and cDNA sequencing.

RSV Recovery, Amplification, and Stability Testing. recRSV stocks were grown on HEp-2 cells inoculated at a multiplicity of infection (MOI) of 0.01 pfu/cell. Infected cells were kept for 16 h at 37 °C, followed by incubation at 32 °C for 5−7 days. Cell-associated progeny virus was released through one freeze/thaw cycle, and titers were determined by $TCID_{50}$ titration on HEp-2 cells. For genetic stability testing of the SMASh-tagged virus, recovered recRSV A2-L19F-fireSMASh virions were consecutively passaged five times on HEp-2 cells. Progeny virions of the second and fifth passage were incubated in the presence or absence of 3 μM asunaprevir (ASV) and infected cell lysates subjected to sodium dodecyl sulfate−polyacrylamide gel electrophoresis (SDS−PAGE) and immunoblotting.

SDS−PAGE and Antibodies. Infected cells (6×10^5 cells/well in a six-well plate format) were lysed 40 h postinfection in RIPA buffer [1% sodium deoxycholate, 1% NP-40, 150 mM NaCl, 50 mM Tris-HCl (pH 7.2), 10 mM EDTA, 50 mM sodium fluoride, protease inhibitors (Roche), and 1 mM phenylmethanesulfonyl fluoride] and subjected to clearance centrifugation (20000*g* for 30 min at 4 °C) and cleared lysates diluted with urea buffer [200 mM Tris (pH 6.8), 8 M urea, 5% sodium dodecyl sulfate (SDS), 0.1 mM EDTA, 0.03% bromophenol blue, and 1.5% dithiothreitol] at a 1:2 ratio. Denatured (30 min at 50 °C) lysates were fractioned through gel electrophoresis on 10% Tris/glycine gels and transferred to polyvinylidene difluoride (PVDF) membranes (GE Healthcare), and protein material was detected through decoration with specific antibodies directed against firefly luciferase (PA5-32209, ThermoFisher) or glyceraldehyde-3-phosphate dehydrogenase (anti-GAPDH, Calbiochem). Immunoblots were developed using mouse IgG light chain-specific HRP-conjugated secondary antibodies (Jackson) and a ChemiDoc digital imaging system (Bio-Rad).

Purification of Virus Stocks. Two alternative strategies were explored to remove contaminating luciferase proteins from virus stocks. Progeny virions in culture supernatants (IAV stocks) or released through one freeze/thaw cycle from infected cells (RSV stocks) were cleared (4000*g* for 20 min at 4 °C) and then pelleted (60000*g* for 30 min at 4 °C). Pelleted material was resuspended in TNE buffer [50 mM Tris-HCl (pH 7.2) and 10 mM EDTA] and purified through a 20%/60% one-step sucrose gradient in TNE buffer (100000*g* for 90 min at 4 °C). Virions were harvested from the gradient intersection. Alternatively, cleared RSV stocks were purified and polished through size exclusion and binding chromatography by being passed through dual-functionality Capto Core 700 resin (GE Healthcare) using an ÄKTA avant chromatography system (GE Healthcare). After purification through either method, virus stocks were stored in aliquots at −80 °C.

Reporter Expression Profiles. Cells (1.5×10^4 per well in a 96-well plate format) were infected with purified virus stocks at different MOIs as specified or co-infected. At the specified time points, cells were lysed *in situ* with 50 μL of Glo-lysis buffer (Promega) for 5 min at 37 °C and samples transferred into solid white 96-well plates. Lysates were kept frozen until the time course was completed and then equilibrated to ambient temperature simultaneously and relative luciferase activities determined using the Synergy H1 reader and injectors to add renilla-Glo, bright-Glo, or dual-Glo substrates (all Promega) (lag time before reading of 3 min for each well). Values are expressed for each reporter strain relative to the highest reading recorded for this strain and represent averages of at least three independent repeats.

Compounds. All compounds were dissolved in DMSO to a concentration of 10 mM and stored at −80 °C. The MScreen software package[40] was used for electronic compound management, HTS data storage, and data analysis. Compounds of the National Institutes of Health (NIH) Clinical Collection (NCC) were received from the NIH Small Molecule Repository in 96-well plates, inventoried in MScreen, and reformatted into barcoded 384-well daughter plates using a Nimbus liquid handler (Hamilton Robotics) with a multichannel pipetting head. In addition, known antimyxovirus bioactives that we have identified in previous drug discovery campaigns were included in empty wells in the NCC daughter plates. Thirty-two wells on each 384-well plate received compound JMN3-003[30] for a positive control, and another 32 wells received volume equivalents of vehicle (DMSO) only. Asunaprevir (ASV) was obtained from Santa Cruz Biotechnology. When included, ASV was added at the time of virus infection.

Assay Validation in 96-Well Format. BEAS-2B cells (2×10^4 cells/well, seeded in 40 μL in white wall/clear bottom 96-well plates) were treated manually (1 μL/well) with a set of known bioactives (diluted in growth medium to 5% DMSO, final concentration as specified) and then infected or co-infected with 10 μL of the IAV and RSV reporter viruses at different MOIs as specified. Final DMSO concentrations were 0.1%, at which no vehicle-induced cytotoxic effect was detected. After a 40 h incubation at 37 °C, luciferase substrates (25 μL/well) were injected as before directly into the assay plates and relative bioluminescence intensities determined. Each compound was assessed in five replicates. For quantitative assay validation, Z' values[41] were calculated according to the formula $Z' = 1 - [3SD_{(C)} + 3SD_{(B)}]/[Mean_{(C)} - Mean_{(B)}]$, where C indicates control and B background.

Automated HTS Protocol in 384-Well Plate Format. BEAS-2B cells (8×10^3 cells/well) were injected (30 μL/well) into barcoded white wall/clear bottom 384-well plates using a

DOI: 10.1021/acs.biochem.5b00623
Biochemistry 2015, 54, 5589−5604

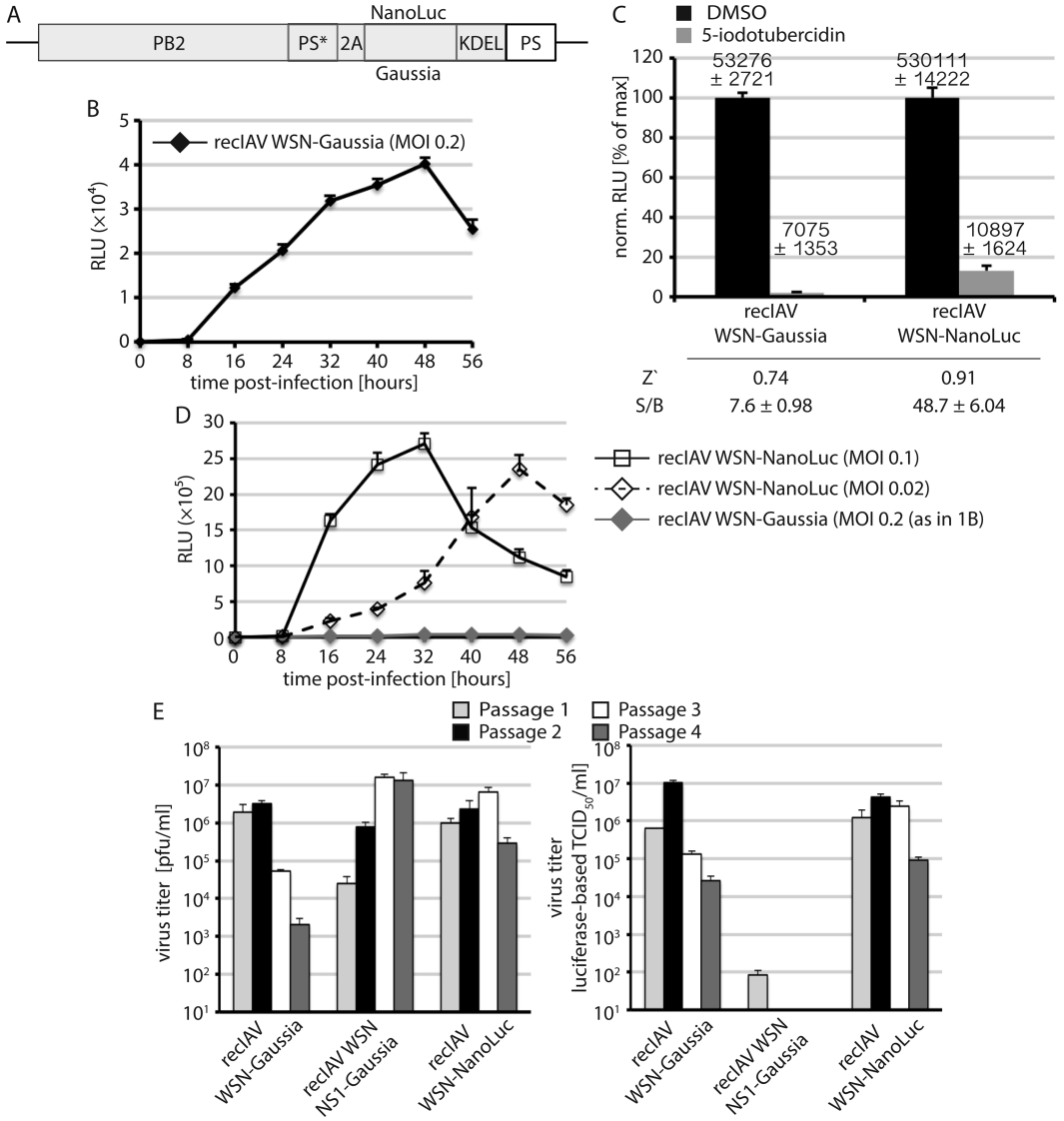

Figure 1. Generation of a recIAV WSN-NanoLuc reporter strain. (A) Schematic of the WSN PB2-NanoLuc or PB2-Gaussia genome segment (PS*, downstream packaging signal that was inactivated through silent mutagenesis; 2A PTV-derived cleavage site; NanoLuc or Gaussia, luciferase ORF; KDEL, ER retention signal; and PS, engineered packaging signal). Gray shading specifies the reading frame of the engineered segment. Individual segments are not drawn to scale. (B) Reporter expression profile of IAV WSN-Gaussia on A549 cells (N = 3; means ± SD are shown). Instrument gain of 250; RLU indicates relative luciferase units. (C) Signal window of the recIAV WSN-Gaussia and analogous recIAV WSN-NanoLuc reporter strains. A549 cells were exposed at infection to the potent inhibitor 5-iodotubercidin[85] at 10 μM or the vehicle (DMSO) volume equivalent. RLUs were determined 48 h postinfection. Values were normalized for vehicle controls (N = 3; means ± SD are shown); numbers above the columns show raw data means ± SD. Z' and S/B values are specified below the graph. (D) Reporter expression profiles of recIAV WSN-NanoLuc as in panel B after infection of A549 cells at two different MOIs (N = 3; means ± SD are shown). Instrument gain of 135 for recIAV WSN-NanoLuc. The IAV WSN-Gaussia profile was added for comparison. (E) recIAV WSN-NanoLuc and WSN-Gaussia are genetically stable over several passages. Progeny viral titers were determined by a plaque assay (left) and $TCID_{50}$ titration using luciferase activity as the read-out (right) after each passage (N = 3; means ± SD are shown).

MultiFlo automated dispenser (BioTek) equipped with dual 10 μL peristaltic pump manifolds, collected (150g for 90 s at 25 °C), and incubated for 5 h at 37 °C and 5% CO_2. Compound was added to a final concentration of 5 μM (20 nL/well) using a high-density pin tool (V&P Scientific) attached to the pipetting head of the Nimbus liquid handler, followed by co-infection with recRSV A2-L19F_{D489E}-fireSMASh (MOI = 0.1) and recIAV WSN-NanoLuc (MOI = 0.02) at a level of 10 μL/well using the MultiFlo dispenser unit, spin collection (150g for 90 s at 25 °C), and incubation for 40 h at 37 °C and 5% CO_2. The final vehicle (DMSO) concentration was 0.05%. Barcodes of source and assay plates were automatically detected and recorded by the Nimbus unit at the time of stamping. Using a stacker unit with an integrated barcode reader (Biotek) attached to the H1 synergy plate reader, plates were automatically loaded, dual-Glo substrates (15 μL/well each) were injected, and bioluminescence was recorded after a 3 min lag time for each well and substrate. Readouts were automatically saved by plate barcode. For manual calculation of Z' values, luciferase activities in positive and vehicle wells were processed as detailed above.

Dose–Response Counterscreens. Twofold serial dilutions of hit candidates were prepared in 384-well plates in three replicates each using the Nimbus liquid handler. BEAS-2B cells

DOI: 10.1021/acs.biochem.5b00623
Biochemistry 2015, 54, 5589–5604

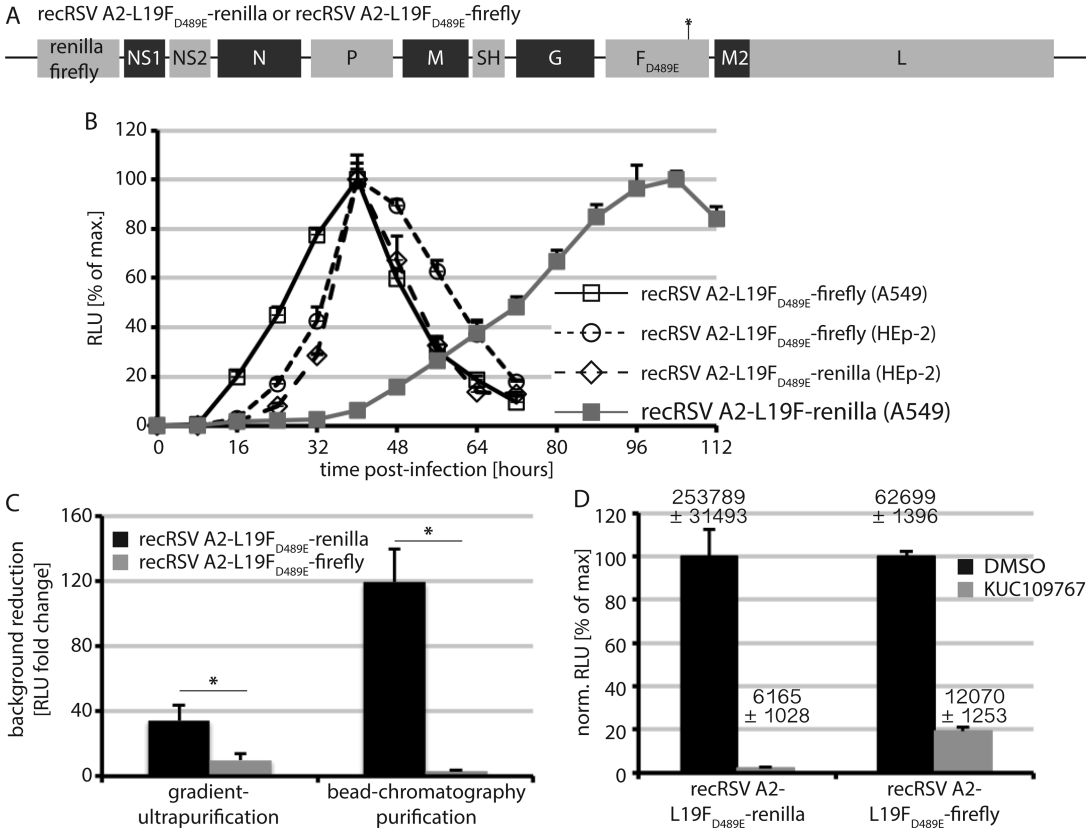

Figure 2. Development of second-generation recRSV reporter strains. (A) Schematic of the recRSV-L19F$_{D489E}$-firefly and Renilla luciferase genomes. (B) Reporter expression profile after infection with recRSV-L19F-renilla or newly generated recRSV-L19F$_{D489E}$-firefly or recRSV-L19F$_{D489E}$-renilla (MOI of 0.3 each; instrument gain of 200). Values represent cell-associated luciferase activities and were normalized to the highest signal of each series ($N \geq 3$; means ± SD are shown). Purification of recRSV-L19F$_{D489E}$-firefly and recRSV-L 19F$_{D489E}$-renilla progeny virions through different techniques. RLUs in virus stocks before and after purification were determined, and background clearance (RLU_{before}/RLU_{after}) was calculated ($N = 3$; means ± SD are shown; two-tailed t test; $^*p < 0.05$). (D) Signal window of the recRSV reporter strains. A549 cells were exposed at infection to 10 μM KUC109767, an inhibitor of RSV RdRp activity,[86] or the vehicle (DMSO) volume equivalent. RLUs were determined 44 h postinfection and values normalized for vehicle controls ($N = 3$; means ± SD are shown); numbers above the columns show raw data means ± SD.

(8×10^3 cells/well) were then plated as before, serial dilutions transferred using the pin tool, and cells infected with recRSV A2-L19F$_{D489E}$-fireSMASh (MOI = 0.1), recRSV A2-L19F-renilla (MOI = 0.1), or recIAV WSN-NanoLuc (MOI = 0.02) or left uninfected for cell viability assessment. Reporter signals were recorded as outlined above. To determine cell viability, PrestoBlue substrate (life technologies) was added after a 40 h incubation of the cells at 37 °C (5 μL/well) and top-read fluorescence (excitation at 560 nm, emission at 590 nm, instrument gain of 85) recorded after incubation for 45 min at 37 °C using the H1 synergy plate reader. Four-parameter variable slope regression modeling was applied to determine 50% active (EC_{50}) and toxic (CC_{50}) concentrations.

Data Normalization and Analysis. The MScreen package was employed for automated data analysis. Plate reader raw data files together with source and assay plate barcode maps generated by the Nimbus system were directly imported into the package, and Z' values were automatically calculated on the basis of the designated control wells. Because the NCC plates contained a high density of known bioactives, the normalized percent inhibition method was applied for data analysis. Normalized relative inhibition values were calculated for each compound by subtracting each value from the average of the plate vehicle controls, followed by dividing the results by the difference between the means of plate vehicle and positive controls. Hit candidates were defined as compounds showing ≥75% inhibition of normalized signal intensity against either viral target or both. For analysis of replicate plates, the cellHTS2 package[42] was employed to calculate percent inhibition as described above, followed by scaling of plates by dividing the normalized value of each well by the median absolute deviation of the plate. Results are given as Z scores, positive Z scores reflecting more potent inhibition. The dynamic range was calculated for each plate as the ratio between the geometric means of the positive and negative controls. The SciFinder database package (American Chemical Society) was used to query chemical databases with hit candidate structures to evaluate known bioactivities.

Statistical Analysis. The Excel and Prism 6 (GraphPad) software packages were used for data analysis. The statistical significance of differences between two sample groups was assessed by an unpaired two-tailed t test (two sample groups; Excel) or two-way analysis of variance (ANOVA; Prism 6) in combination with Tukey's multiple-comparison post-tests (multiple sample groups) as specified in the figure legends. Experimental uncertainties are identified by error bars, representing standard deviations (SD).

RESULTS

Different versions of replication-competent IAV strains encoding luciferase reporters were described recently.[35,43] Of

DOI: 10.1021/acs.biochem.5b00623
Biochemistry 2015, 54, 5589−5604

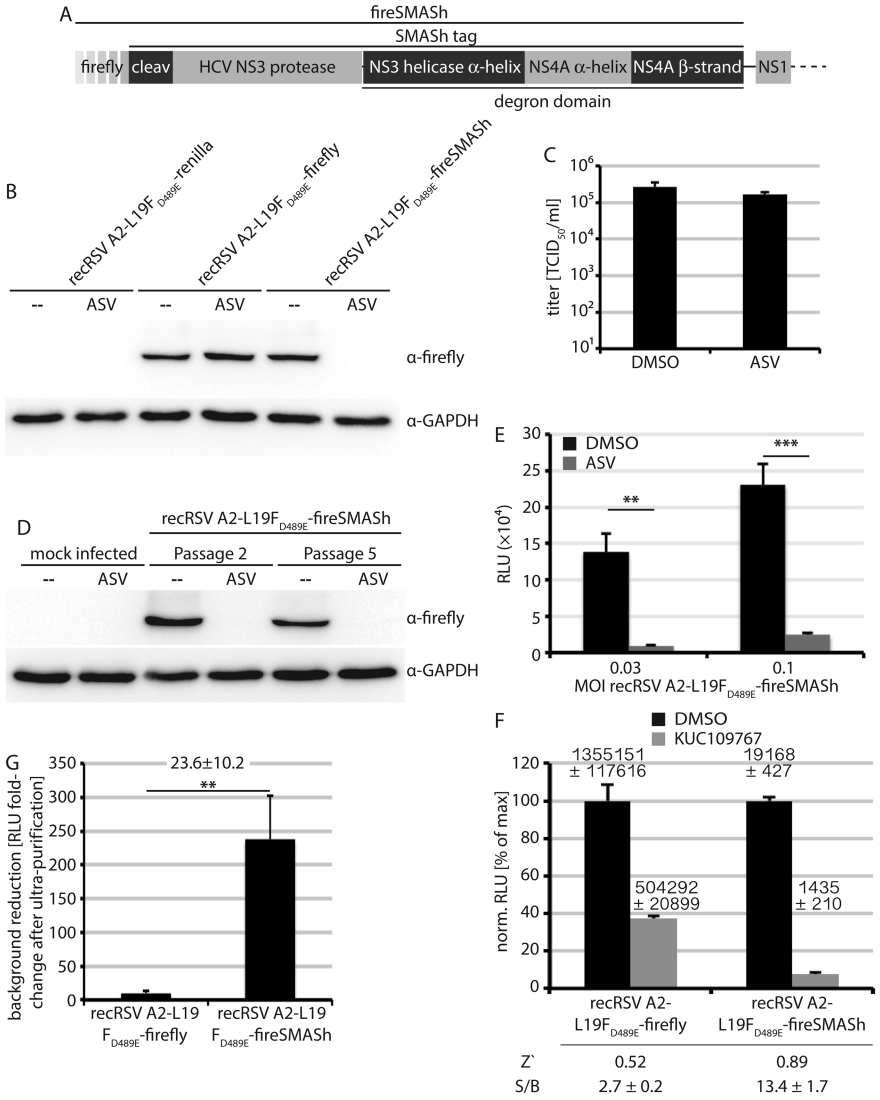

Figure 3. recRSV-L19F$_{D489E}$-fireSMASh allows induced reporter degradation. (A) Schematic of the fireSMASh cassette inserted into the recRSV-L19F$_{D489E}$ genome (cleav, HCV NS3 cleavage site). (B) Immunodetection of firefly luciferase after infection of cells with the specified recRSV-L19F$_{D489E}$ strain in the presence or absence of the NS3 inhibitor asunaprevir (ASV) and SDS−PAGE of cell lysates. Cellular GAPDH levels were determined as loading controls. (C) Peak recRSV-L19F$_{D489E}$-fireSMASh progeny titers after incubation in the presence of 3 μM ASV or vehicle (DMSO) (N = 3; means ± SD are shown). (D) Immunodetection of firefly luciferase after serial passaging of recRSV-L19F$_{D489E}$-fireSMASh and re-infection of cells in the presence or absence of 3 μM ASV. Passage 2 (P2) and passage 5 (P5) are shown, and GAPDH levels were determined as loading controls. (E) Firefly activity after growth of recRSV-L19F$_{D489E}$-fireSMASh in the presence or absence of 3 μM ASV. Cells were infected at the specified MOIs and harvested 44 h postinfection (N = 3; means ± SD are shown; two-tailed t test, $^{**}p < 0.01$; $^{***}p < 0.001$). (F) The signal window of the recRSV-L19F$_{D489E}$-fireSMASh reporter strain was calculated as described in Figure 2D (N = 3; means ± SD are shown); numbers above the columns show raw data means ± SD. Z' and S/B values are specified below the graph. (G) Fold change of contaminating firefly luciferase after gradient purification of recRSV-L19F$_{D489E}$-firefly and recRSV-L19F$_{D489E}$-fireSMASh preparation to unpurified recRSV-L19F$_{D489E}$-firefly (N = 3; means ± SD are shown; two-tailed t test; $^{**}p < 0.01$).

these, a recombinant IAV-PR8 harboring a Gaussia open reading frame in the PB2 genome segment reportedly replicated efficiently, was genetically stable, and showed high luciferase activity levels.[35]

Generation of a Replication-Competent IAV-WSN PB2-NanoLuc Reporter Strain. Most laboratory IAV strains require the addition of exogenous trypsin for proteolytic maturation of the HA protein for priming of the viral entry machinery. To gain independence of trypsin activation in all screening plates, we generated the analogous PB2-Gaussia recombinant in the trypsin-independent IAV-WSN genetic background (Figure 1A).[44] The resulting recIAV-WSN Gaussia showed efficient replication and reporter expression in the absence of exogenous trypsin (Figure 1B). However, the signal window of Gaussia remained below 10 (Figure 1C). With respect to extending the assay range, we substituted Gaussia luciferase for the recently developed nanoluciferase [NanoLuc (Figure 1A)], which uses the same basic substrate chemistry as Gaussia and Renilla luciferases but combines a small protein size with high signal intensities. Recovered recIAV-WSN NanoLuc indeed returned a >6-fold improved signal window and showed superior absolute luciferase signal intensities compared to those of recIAV-WSN Gaussia (Figure 1C,D). Z' values in either case far exceeded 0.5, suggesting that the assay is suitable for automation. Serial passaging of this recombinant confirmed the equivalent genetic stability of

DOI: 10.1021/acs.biochem.5b00623
Biochemistry 2015, 54, 5589−5604

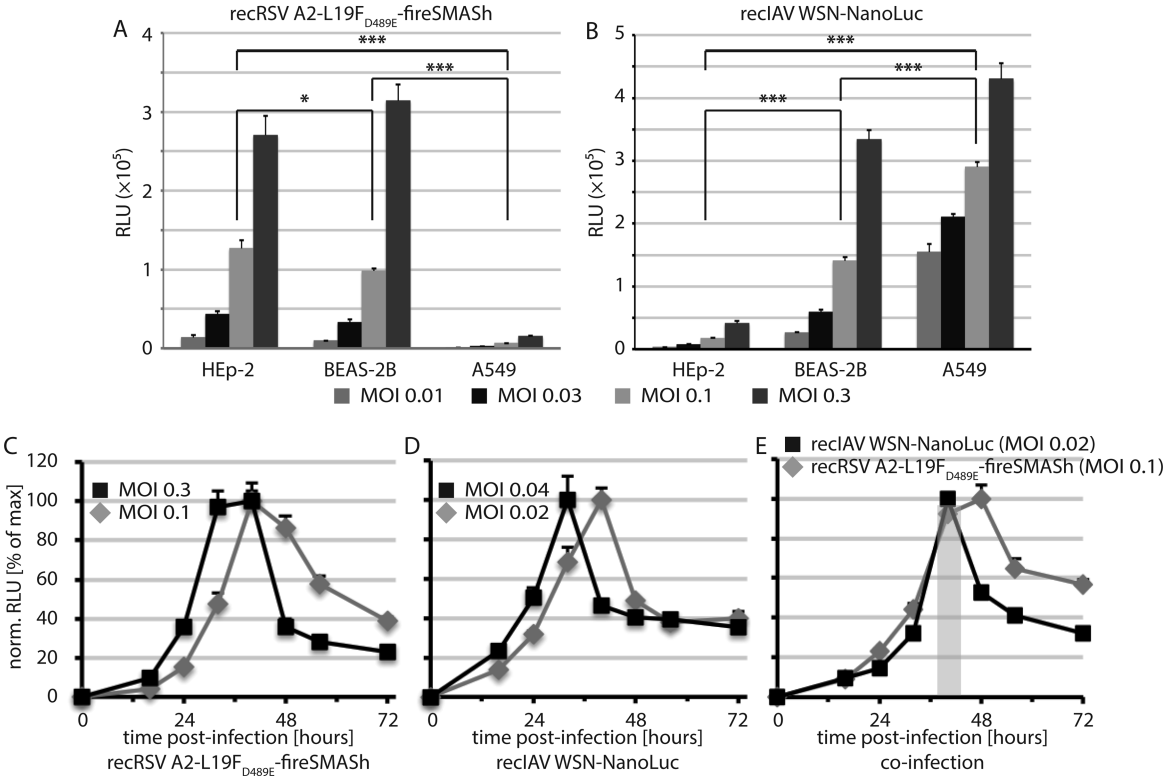

Figure 4. Infection conditions for synchronized RSV and IAV reporter expression. (A and B) Luciferase activities in three different human respiratory host cell lines 44 h postinfection at the specified MOIs with recRSV-L19F$_{D489E}$-fireSMASh (A) or recIAV WSN-NanoLuc (B; N = 4; means ± SD are shown). Two-way ANOVA with Tukey's multiple-comparison post-tests were conducted to assess the statistical significance of sample divergence. Results are shown for MOIs of 0.1 (A) and 0.04 (B); *p < 0.05; ***p < 0.01. (C–E) Reporter activity profiles after infection of BEAS-2B cells singly with recRSV-L19F$_{D489E}$-fireSMASh (C) or recIAV WSN-NanoLuc (D), or after co-infection with both strains at MOIs of 0.1 (RSV) and 0.02 (IAV), respectively (E). Values represent cell-associated luciferase activities and were normalized to the highest-intensity signal of each series (N = 3; means ± SD are shown). The gray shaded area in panel D marks the time window postinfection when signal intensities of both luciferase reporters are ≥80% of the maximum.

recIAV-WSN Gaussia and recIAV-WSN NanoLuc. By comparison, luciferase activity rapidly disappeared when a recIAV-WSN NS-Gaussia was subjected to passaging, which harbors the luciferase open reading frame in the NS genome segment (Figure 1E). The design of this recombinant followed the strategy outlined in a recent report.[36]

An IAV-Compatible Recombinant RSV-Firefly Reporter Strain. In the original evaluation of a dual-myxovirus HTS protocol, we found that IAV- and MeV-based reporter expression overlapped, whereas the original recRSV-L19F-renilla reporter strain showed a substantial delay in luciferase expression over a range of different inoculum multiplicities of infection (MOIs). Upon comparison of RSV and MeV in a cell culture, most notable is the divergence in cell-to-cell fusion (syncytia formation) after infection, which represents the hallmark of MeV cytopathicity but is much less pronounced in the case of RSV. We therefore hypothesized that the lower rate of lateral RSV spread may cause the slower reporter expression kinetics and asked whether a hyperfusogenic RSV variant would alleviate the problem. We have previously generated an RSV recombinant with a D to E substitution of fusion (F) protein residue 489 that renders it hyperfusogenic.[45]

To test the effect of hyperfusogenicity on reporter expression kinetics, we generated a recRSV-L19F$_{D489E}$-firefly strain (Figure 2A) analogous to the previously described recRSV-L19F-renilla strain, because firefly and nanoluciferase activities are based on distinct substrate chemistry and can be independently quantified. Independent of the nature of the luciferase reporter included, the time to peak reporter activity of F$_{D489E}$ mutant strains was less than half of that of a strain harboring standard F (Figure 2B). These results suggest that the hyperfusogenic recRSV-L19F$_{D489E}$-firefly strain should be suitable for co-infection screens with recIAV WSN-NanoLuc. When attempting to purify recRSV-L19F$_{D489E}$-firefly preparations from contaminating firefly protein that was synthesized during stock growth, however, we noted that both gradient ultracentrifugation and layered bead chromatography purification strategies successfully reduced the levels of Renilla luciferase contamination but by comparison remained inefficient against firefly luciferase (Figure 2C). As a consequence, the signal window of assays based on the recRSV-L19F$_{D489E}$-firefly strain was approximately 8-fold lower than that which can be achieved with recRSV-L19F$_{D489E}$-renilla (Figure 2D), excluding its use in high-density HTS applications.

SMASh Technology for Eliminating Contaminating Firefly Protein. In search of an innovative approach to suppress the buildup of contaminating firefly protein during growth of virus stocks, we explored the use of small-molecule-assisted shut-off (SMASh) technology for induced protein degradation that we have recently developed.[39] Unlike other systems designed to induce protein turnover, only SMASh functions as a single-chain system and in the stabilized state returns near-native proteins. Added as a genetic tag, SMASh consists of a hepatitis C virus-derived NS3 protease flanked by a

DOI: 10.1021/acs.biochem.5b00623
Biochemistry 2015, 54, 5589–5604

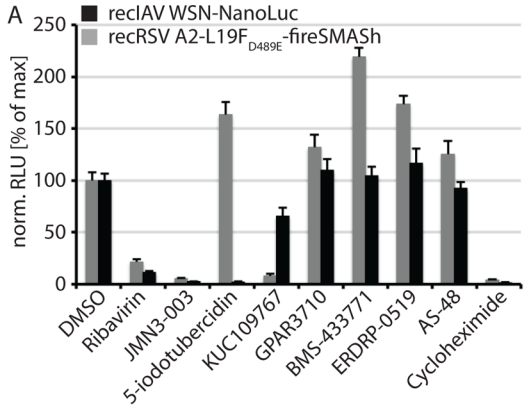

B

format	approach	reporter virus strain	S/B	Z`	AVR dynamic range
96-well	manual	recRSV A2-L19F$_{D489E}$-fireSMASH	20.0 ± 5.6	0.67	ND
		recIAV WSN-NanoLuc	41.0 ± 8.0	0.68	ND
384-well	automated	recRSV A2-L19F$_{D489E}$-fireSMASH	53.9 ± 3.4	0.54	3.98
		recIAV WSN-NanoLuc	22.5 ± 4.8	0.63	6.03

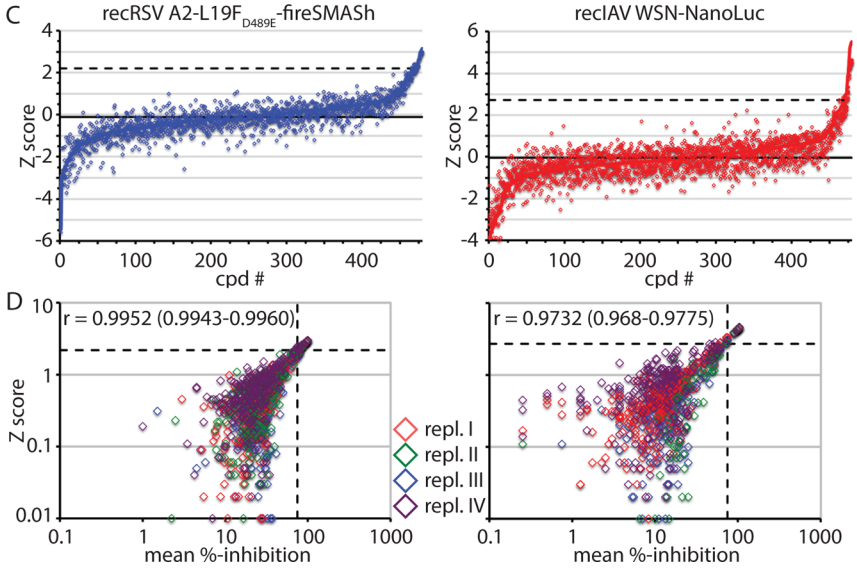

Figure 5. Assay miniaturization and validation. (A) Co-infection of BEAS-2B cells with recRSV-L19F$_{D489E}$-fireSMASh and recIAV WSN-NanoLuc as specified in Figure 4E in a 96-well plate format. Known RSV-specific [KUC109767 (10 μM),[86] GPAR3710 (10 μM),[87] and BMS-433771 (10 μM)[48]], IAV-specific [5-iodotubercidin (10 μM)[85]], and MeV-specific [ERDRP-0519 (10 μM)[88] and AS-48 (40 μM)[89]] inhibitors, broad-spectrum antivirals [ribavirin (40 μM) and JMN3-003 (10 μM)[30]], and cytotoxic cycloheximide (100 μg/mL) were used for assay validation (N = 5; means ± SD are shown). (B) Co-infection assay parameters obtained in 96-well (manual; one plate each; N = 5; means ± SD are shown) and 384-well (automated; four plates each; N = 128; means ± SD are shown) format. The broad-spectrum myxovirus inhibitor JMN3-003[30] was used as a reference compound. AVR dynamic range, mean dynamic range across all replicate plates; ND, not determined. (C) Z score profiles of automated dual-pathogen pilot screens of the NCC collection in 384-well plate format in four replicates. Symbols mark Z scores of individual replicate screens; solid black lines represent the assay Z score mean, and dashed black lines show the hit cutoff [assay mean + 2.5 × (assay Z score SD)]. The final screening concentration was 5 μM. (D) Individual Z scores of the replicate (repl. I–IV) screens shown in panel C are plotted as a function of the mean percent inhibition for each compound. Dashed horizontal and vertical black lines show hit cutoffs based on Z score [assay mean + 2.5 × (assay Z score SD)] and biological effect (mean inhibition of >75%), respectively. Numbers represent Pearson correlation coefficients (r) and 95% confidence intervals.

strong degron domain inducing proteasomal degradation. An NS3 protease site is positioned at the intersection of the SMASh tag and the target protein (Figure 3A). Under normal conditions, NS3 autoproteolysis separates the tag, returning the near-native target protein. In the presence of a strong NS3 inhibitor such as the clinical candidate ASV,[46] however, autoproteolysis is blocked and the degron domain induces rapid degradation of the tag and affixed target protein.

We added a SMASh tag to the firefly open reading frame and successfully recovered the corresponding recRSV-L19F$_{D489E}$-fireSMASh recombinant. Immunoblotting with antibodies directed against firefly luciferase confirmed efficient degradation of the tagged protein after incubation in the presence of ASV, while steady state levels closely matched those of untagged firefly luciferase in the absence of the drug (Figure 3B). As expected, ASV had no effect on progeny virus titers (Figure

DOI: 10.1021/acs.biochem.5b00623
Biochemistry 2015, 54, 5589–5604

Table 1. Primary Screening Hit Candidates of the NCC, Based on Automated Screening of the Library in Four Replicates in 384-Well Format[a]

name	% inhibition (anti-RSV)[b]	% inhibition (anti-IAV)[b]	bioactivity/biological target[c]	known antiviral targets[c]
			RSV Predominant	
Temozolomide	96 ± 1.3	55 ± 3.2	DNA replication[69]	none
Raltiterxed	91 ± 1.0	60 ± 6.5	thymidylate synthase[70]	cytomegaloviruses[70]
Rosiglitazone	85 ± 5.8	35 ± 5	adenomatosis polyposis coli 2 eukaryotic translation initiation factor 5A-1 peroxisome proliferator-activated receptor-γ[71]	rotaviruses[71]
etoposide	80 ± 6.6	56 ± 5.6	DNA topoisomerase II[72]	cytomegaloviruses[72]
eincristine	79 ± 6.9	50 ± 2.9	microtubule assembly[73]	none
			IAV Predominant	
Actinomycin D	52 ± 9.6	104 ± 1.5	RNA synthesis[74]	reovirus type 2[74]
Triptolide	1.5 ± 21	103 ± 1.2	XPB (a subunit of TFIIH)[75]	HIV-1[75]
Epirubicin	62 ± 6.3	75 ± 3.1	DNA intercalator 104	hepatitis C[76]
			Inhibition of Both Reporter Strains	
Methotrexate	99 ± 0.5	100 ± 0.6	dihydrofolate reductase, deoxycytidine kinase[58]	murine and human cytomegalovirus[58]
Homoharringtonine	98 ± 0.5	90 ± 2.6	60S ribosome inhibitor[77]	recombinant murine coronavirus[77]
Idarubicin	95 ± 1.3	97 ± 1	DNA topoisomerase II[78]	encephalomyocarditis virus (EMCV)[78]

[a]Results are grouped by RSV-specific hit candidates, IAV-specific hit candidates, and inhibitors of both target viruses. [b]Based on four independent replicate screens; mean % inhibition ± SD are shown. [c]Previously proposed activity, target, and antiviral spectrum, if known.

3C), and the SMASh tag remained stable over multiple passages of this virus strain (Figure 3D). However, growth of recRSV-L19F$_{D489E}$-fireSMASh in the presence of ASV reduced firefly luciferase activity by approximately 90% (Figure 3E), which paved the path for improved assay performance (Figure 3F) and a >23-fold increased signal window of recRSV-L19F$_{D489E}$-fireSMASh compared to that of recRSV-L19F$_{D489E}$-firefly (Figure 3G). These results suggest that recIAV WSN-NanoLuc and recRSV-L19F$_{D489E}$-fireSMASh may represent a suitable pair for dual-pathogen drug discovery campaigns.

Co-Infection Conditions. To establish suitable assay conditions, we first independently infected three human respiratory cell lines, HEp2, BEAS-2B, and A549, with recRSV-L19F$_{D489E}$-fireSMASh and recIAV WSN-NanoLuc at different multiplicities of infection and measured relative luciferase activities 40 h postinfection to test for the host cell preference of the reporter strains. At each MOI, the level of RSV-based reporter expression was reduced in A549 cells by >90% compared to those of each of the other two cell lines (Figure 4A), and a comparable reduction was observed with IAV-based NanoLuc expression in HEp2 cells (Figure 4B).

We therefore selected BEAS-2B cells as being best suited for RSV/IAV co-infection experiments and generated reporter expression profiles after infection with either virus individually (Figure 4C,D) or in combination (Figure 4E). Peak luciferase activities (RLUs ≥ 80% of the maximum) overlapped in an approximately 7 h time window (37−44 h postinfection) when cells where co-infected with recRSV-L19F$_{D489E}$-fireSMASh at an MOI of 0.1 and recIAV WSN-NanoLuc at an MOI of 0.02. All subsequent experiments followed these assay conditions, and reporter signals were measured 38−42 h postinfection.

Assay Miniaturization and Validation. With respect to validating the assay for screening campaigns, we initially applied the protocol in 96-well plate format to a panel of known bioactives with discrete antimyxovirus activity and cytotoxic compounds for comparison (Figure 5A). Relative inhibition was calculated through normalization of raw data for control wells that received vehicle (DMSO) only. In all cases, known myxovirus inhibitors with different antiviral profiles were correctly identified, and Z' values (Figure 5B) exceeded 0.5, defining a robust assay.[47] The previously characterized RSV fusion blockers GPAR3710 and BMS-433771[45,48] did not emerge as hits, confirming our hypothesis that the use of the pan-resistant RSV-F$_{D489E}$ mutant will reliably suppress the discovery of additional, undesirable RSV entry inhibitors that are also sensitive to the pan-resistance escape mechanism that we have recently described.[45]

On the basis of this proof-of-concept data, we miniaturized the assay to 384-well plate format and screened a two-plate pilot set of the National Compound Collection (NCC) in quadruplicate to quantify assay suitability for automated hit discovery and determine plate-to-plate and day-to-day reproducibility. In addition, we added previously identified broad-spectrum myxovirus inhibitors[30] to the NCC set for reference. Executed under HTS conditions, this validation campaign returned robust Z' values exceeding 0.5 and signal windows greater than 50 for RSV and 20 for IAV (Figure 5B).

Of the NCC test library, 11 hit candidates that inhibited primary reporter activities by ≥75% of either target virus or both were identified (Table 1). The majority of these hit candidates were previously associated with diverse antiviral and/or cytotoxic activities. Graphic representation of all assay validation replicates in Z score profiles revealed that the dual myxovirus protocol shows high plate-to-plate reproducibility (Figure 5C). Plotting of individual Z scores of each replicate as a function of mean percent inhibition values for each compound and viral target furthermore revealed a strong correlation between normalized scores and effect sizes for all hit candidates (Figure 5D).

Test Screen of a 1280-Compound Library. For a proof of concept of hit identification under single-replicate screening conditions, we applied the validated assay to the LOPAC1280 library of pharmacologically active compounds (Figure 6A). This campaign yielded 24 primary hit candidates (1.875% hit rate). Positives included, among others, known anti-influenza virus and anti-RSV inhibitors (Zanamivir and Ribavirin), protein biosynthesis blockers (i.e., Emetine), and DNA/RNA synthesis inhibitors (i.e., PMEG and Idarubicin) (Table 2). Of

DOI: 10.1021/acs.biochem.5b00623
Biochemistry 2015, 54, 5589−5604

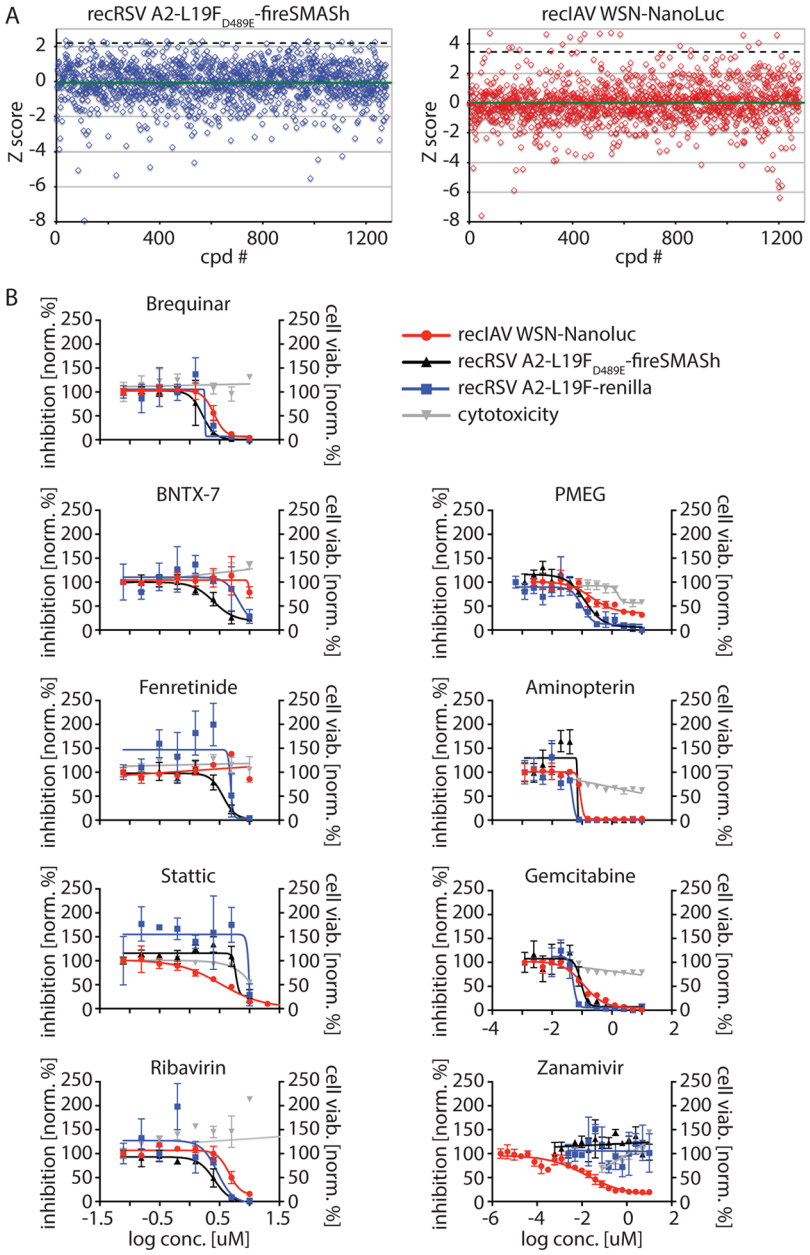

Figure 6. Test screen of a 1280-compound LOPAC library of known bioactives (overall Z' = 0.31). (A) Z score profiles of the automated proof-of-concept screen of the LOPAC library in 384-well format. Solid green lines show Z score means and dashed black lines hit cutoffs [assay mean + 2.0 × (assay Z score SD) for recRSV A2-L19F$_{D489E}$-fireSMASh and assay mean + 2.5 × (assay Z score SD) for rec IAV WSN-NanoLuc]. The final screening concentration was 5 μM. (B) Dose−response assays of hit candidates in a concentration (conc.) range of 10−0.078 or 10−0.0006 μM. Only hits with CC_{50} values of ≥10 μM and confirmed inhibition of at least one primary target virus are shown. Values were normalized (norm.) for vehicle (DMSO)-treated infections and represent mean percent inhibition or percent cell viability (viab.) of three replicates ± SD. Regression curves for antiviral (black) or cytotoxic (gray) activities are based on four-parameter modeling where applicable.

note, Zanamivir, Ribavirin, and Amantidine were the only antiviral drugs in this library licensed for the treatment of IAV and/or RSV infections. Because the recIAV-WSN strain used for screening is resistant against the M2 channel blocker amantadine, the assay correctly identified all licensed therapeutics with antimyxovirus indication.

All compounds were picked (Table 2 and Table S1) and subjected to cytotoxicity testing. Only candidates that reduced cell viability by <50% at twice the screening concentration (10 μM) were admitted to automated dose−response testing [14 compounds (Table 2)] against the primary screening strains. Interference with the luciferase reporter or the NS3 protease activity of the SMASh tag was addressed in parallel by testing against a standard recRSV A2-L19F reporter strain lacking the F_{D489E} resistance mutations and expressing Renilla luciferase that does not share substrate chemistry with firefly luciferase.[38] Compound interference with nanoluciferase is addressed by testing against cells transiently transfected with a nanoluciferase expression plasmid in our confirmation pipeline, but we did not implement this counterscreen in this exercise because only the licensed influenza drug Zanamivir selectively inhibited the IAV reporter. Whenever possible, 50% active and cytotoxic concentrations of the selected hit candidates were calculated

DOI: 10.1021/acs.biochem.5b00623
Biochemistry 2015, 54, 5589−5604

Table 2. Dose−Response Counterscreening of Hit Candidates Identified through Automated Screening of the LOPAC1280 Library in a Single Replicate in 384-Well Format

name	EC_{50}[a] IAV WSN-nanoLuc (μM)	EC_{50}[a] RSV A2-L19F-renilla (μM)	EC_{50}[a] RSV A2-L19F$_{D489E}$-fireSMASh (μM)	CC_{50}[a] (PrestoBlue cell viability) (μM)	proposed target/bioactivity	SI (CC_{50}/EC_{50}), comment
Aminopterin	0.09 (0.07−0.11)	0.05 (0.03−0.07)	0.07	10	dihydrofolate reductase/purine synthesis	SI_{IAV} 111 SI_{RSV} 143 conf. broad spectrum[79,80]
Brequinar	2.6 (2.3−2.9)	1.8	1.6 (1.3−2.1)	>10[b]	DHODH/pyrimidine synthesis	SI_{IAV} >3.8 SI_{RSV} >6.3 conf. broad spectrum[81,82]
Gemcitabine	0.1 (0.09−0.14)	0.05 (0.04−0.06)	0.09 (0.07−0.12)	>10	nucleoside analogue	SI_{IAV} >100 SI_{RSV} >111 HIV, IAV[49,50]
Zanamivir	0.02 (0.01−0.04)	inactive	inactive	>10[b]	neuraminidase	SI_{IAV} >500 IAV inhibitor[83]
Calcimycin	nd[c]	nd[c]	nd[c]	tox[d]	cation ionophore	tox discarded
Emetine	nd[c]	nd[c]	nd[c]	tox[d]	ribosome	tox discarded
ET-18-OCH3	inactive[e]	inactive[e]	inactive[e]	>10[b]	PIPLC/PKC	failed conf.
Sunitinib	nd[c]	nd[c]	nd[c]	tox[d]	RTKs	tox discarded
Idarubicin	nd[c]	nd[c]	nd[c]	tox[d]	topoisomerase	tox discarded
Fenretinide	inactive[e]	4.8	3.6 (2.9−4.6)	>10[b]	activation of stress kinases; induces autophagy	SI_{RSV} >2.8 Dengue,[62] HIV[61]
BNTX-7	inactive[e]	6.5 (0.14−307)	2.5 (1.8−3.6)	>10[b]	DOR1	SI_{RSV} >4
Lometrexol	nd[c]	nd[c]	nd[c]	tox[d]	purine synthesis	tox discarded
PMEG	0.2 (0.1−0.4)	0.1 (0.07−0.15)	0.1 (0.09−0.18)	10	acyclic nucleotide analogue	SI_{IAV} 50 SI_{RSV} 100 HPV[67]
Nitrendipine	inactive[e]	inactive[e]	inactive[e]	>10[b]	dihydropyridine calcium channel	failed conf.
PD173952	nd[c]	nd[c]	nd[c]	tox[d]	Src kinase	tox discarded
K114	inactive[e]	inactive[e]	inactive[e]	>10[b]	amyloid-specific dye	failed conf.
Phenanthroline	nd[c]	nd[c]	nd[c]	2.4[d]	metalloproteases	tox discarded
Auranofin	nd[c]	nd[c]	nd[c]	tox[d]	TLR signaling	tox discarded
Sanguinarine	nd[c]	nd[c]	nd[c]	tox[d]	Na/K ATPase	tox discarded
Stattic	3.3 (2.2−5.1)	15.1	5.9	10	STAT3	SI_{IAV} 3
PD-166285	nd[c]	nd[c]	nd[c]	tox[d]	RTKs	tox discarded
Ribavirin	4.5 (2.9−5.3)	2.9 (1.6−5.4)	2.6 (2.1−3.2)	>10[b]	nucleoside analogue	SI_{IAV} >2.2 SI_{RSV} >3.9 broad spectrum[84]
Triamterene	inactive[e]	inactive[e]	inactive[e]	>10[b]	epithelial Na^+ channel	failed conf.
BIX 01294	inactive[e]	inactive[e]	inactive[e]	>10[b]	histone methyltransferase	failed conf.
Triptolide	0.15 (0.11−0.21)	0.6	0.4 (0.3−0.5)	0.3 (0.22−0.4)	XPB (a subunit of TFIIH)	tox discarded

[a]Calculated through four-parameter variable slope regression modeling. Raw values are based on luciferase reporter expression and represent means of three independent replicates. Calculated EC_{50} concentrations and 95% confidence intervals are shown. [b]The highest concentration assessed was 10 μM. [c]Not determined on the basis of initial cell viability testing. [d]Less than 50% cell viability after exposure of cells for 44 h at ≤10 μM. [e]Less than 50% reduction in the intensity of the mean reporter signal.

for all assay targets through four-parameter variable slope regression modeling (Table 2).

Triptolide of the NCC test set originally demonstrated preferential activity against the IAV reporter strain and was likewise selected for dose−response testing and sourced. Of the 15 resulting candidates, five showed only a marginal inhibitory effect against the primary screening strains or were inactive, and Triptolide returned an SI (CC_{50}/EC_{50}) value of <2 at dose−response testing. The remaining nine viable primary hits blocked preferentially either RSV (two compounds) or IAV (two compounds) reporter expression or suppressed both reporter strains (five compounds) (Figure 6B).

First inspection reveals that these confirmed hits can be classified into three distinct groups: (i) licensed antiviral therapeutics such as Zanamivir and Ribavirin, (ii) compounds with documented broad-spectrum antiviral activity such as the nucleoside analogue Gemcitabine[49,50] and inhibitors of the purine and pyrimidine biosynthesis pathways such as Aminopterin and Brequinar, respectively,[51,52] and (iii) compounds not yet extensively associated with antiortho- or paramyxovirus

DOI: 10.1021/acs.biochem.5b00623
Biochemistry 2015, 54, 5589−5604

activity [Fenretinide, BNTX-7, and PMEG hydrate (Table 2)]. Of these, Fenretinide and BNTX-7 selectively inhibited RSV, while the IAV reporter strain was unaffected at the highest concentration tested. PMEG hydrate blocked both reporter strains, although the potency against RSV was approximately 2-fold higher than against IAV.

These results demonstrate that the new generations of recombinant RSV and IAV reporter strains generated in this study can be combined in a robust screening protocol miniaturized to 384-well format. The assay successfully identifies licensed therapeutics and compounds with known antimyxovirus activity. A set of RSV inhibitors merits further mechanistic evaluation.

DISCUSSION

In this study, we have developed and validated a dual-pathogen myxovirus HTS protocol that uses innovative protein engineering technology for the simultaneous discovery of pathogen-specific and broad-spectrum hit candidates (Figure 7). There are several major advantages of this protocol over traditional single-pathogen screens and a first-generation co-infection screen that we have reported previously.[32] (i) Compared to consecutive screening of a library against individual viral targets, the dual-pathogen protocol using replication-competent recombinant viruses shows superior cost and resource effectiveness. (ii) The screening agents used in the new approach, IAV and RSV, are clinically the most significant members of the myxovirus families. (iii) In addition to identifying broad-spectrum blockers, the dual-readout strategy creates a bona fide "internal standard" for each well, excluding cytotoxic and undesirable promiscuous compounds effectively from the pool of virus-specific hit candidates at the stage of primary screening. (iv) The new assay is not systemically restricted in host cell range, but applicable to all cell lines permissive for IAV and RSV replication, including human respiratory epithelial cells. (v) The current assay is suitable for multiple cycle infections, providing flexibility in the choice of inoculum MOI and allowing the interrogation of all stages of the viral life cycle.

Three generations of HTS reporter assays were developed in recent years for the identification of novel influenza virus inhibitors.[53] First-generation assays employed influenza virus-activated reporters; second-generation systems are based on recombinant virions in which one of the viral open reading frames is substituted for a reporter gene, and third-generation influenza virus reporter strains harbor the reporter as additional genetic information in one of the genome segments. Compared to traditional cell-based anti-influenza virus HTS screens that in the majority of cases simply monitor virus-induced cytotoxicity, common advantages to these reporter assays are the quantitative readout, the possibility for assay miniaturization beyond 96-well plate scale, and the higher accuracy of hit identification.

However, first-generation assays require the labor- and resource-intensive preparation of target cell populations and support only single-cycle infections. Both first- and second-generation assays are restricted by a narrow range of suitable target cell lines. By contrast, third-generation influenza virus reporter assays combine high signal intensities with broad target cell flexibility. We therefore explored this strategy and found that the recently developed nanoluciferase technology is particularly suitable for influenza reporter virus HTS applications due to their small size and superior signal

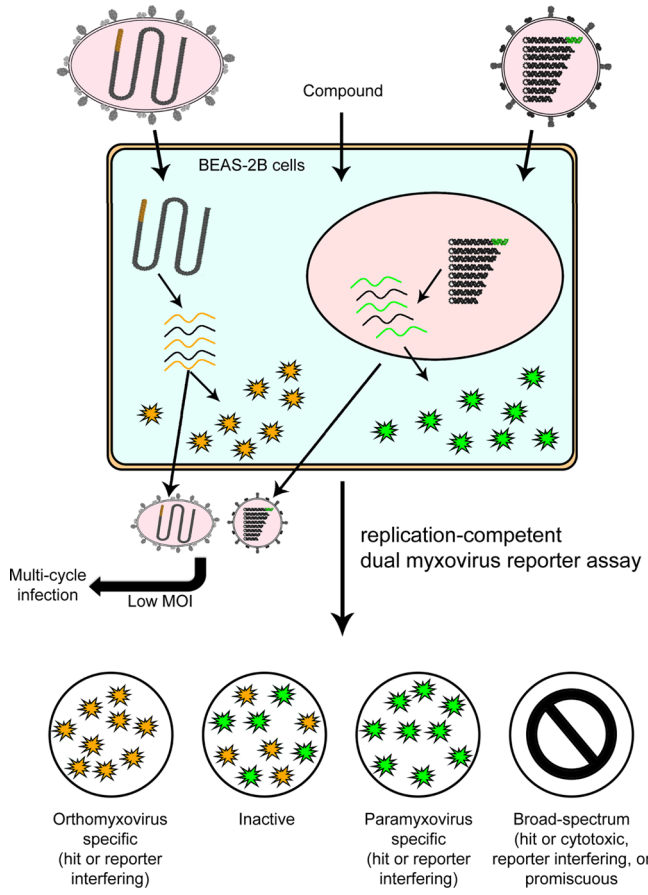

Figure 7. Overview of the replication-competent IAV and RSV reporter strain-based next-generation dual-pathogen HTS protocol for the simultaneous identification of IAV-specific, RSV-specific, and broad-spectrum inhibitors. The assay is validated for human respiratory BEAS-2B cells but can be adapted to all cell lines that are permissive for either virus strain. Infection at a high MOI will predominantly identify inhibitors of viral entry and polymerase, while low-MOI multicycle infections allow interrogation of all stages of the viral live cycle. Counterscreens are required to distinguish between hit candidates or reporter interfering compounds (specific antiviral activity), and hit candidates, reporter interfering compounds, cytotoxic compounds, or promiscuous pan-assay interfering (PAIN) compounds (broad-spectrum activity).

intensities, which translate into robust assay parameters. Naturally, primary screening hits blocking the recIAV WSN-NanoLuc reporter strain must be counterscreened against a panel of currently circulating IAV strains of different genotypes to assess the full anti-IAV indication spectrum.

Our study spotlights that the introduction of the hyperfusogenic F_{D489E} mutation[45] into the RSV reporter strain accelerates the luciferase expression kinetics to a level that we previously observed only with MeV reporter strains.[32] Although MeV and RSV represent distinct paramyxovirus subfamilies, there is little reason to assume that the difference in reporter expression kinetics between RSV and MeV strains is due to substantially faster entry of MeV or slower gene expression of RSV compared to that of MeV. Our results rather indicate that the enhanced cell-to-cell fusion activity of the mutant RSV reporter strain and, thus, accelerated lateral spread through the cell monolayer,[45] altered the reporter expression profile.

We have previously reported that the F_{D489E} mutation causes RSV pan resistance against all known and characterized small-

DOI: 10.1021/acs.biochem.5b00623
Biochemistry 2015, 54, 5589−5604

molecule RSV entry inhibitors, including those currently considered for clinical use.[54−56] The advantage of engineering the F_{D489E} substitution into the screening strain is therefore twofold; first, hyperfusogenicity contributes to synchronizing IAV and RSV reporter expression profiles, and second, the mutation should efficiently suppress the discovery of additional RSV entry inhibitors that are likewise sensitive to the pan-resistance mechanism and have therefore little clinical potential. Consistent with this hypothesis, known RSV entry inhibitors that were spiked into the proof-of-concept screening library did not emerge as hit candidates in our assay validation screens.

Fluorescent recombinant RSV reporter strains were generated more than a decade ago,[57] but we only recently pioneered the application of luciferase reporter technology to the RSV system through the recovery of a recRSV A2-L19F-renilla reporter strain.[38] Because Gaussia luciferase, Renilla luciferase, and nanoluciferase depend on the same substrate chemistry and the small nanoluciferase ORF was most suitable for stable incorporation into a recombinant influenza virus strain, co-infection screening demanded the development of an RSV firefly reporter strain for combination with recIAV WSN-NanoLuc. Virus recovery was straightforward, but high levels of contaminating firefly luciferase protein in virus stocks despite extensive purification of virus preparations prohibited assay miniaturization because of unacceptably low *S*/*B* ratios.

Remarkably, this problem did not surface in earlier work using the recRSV A2-L19F-renilla reporter.[32] Two explanations for the variation in purification success are conceivable; firefly but not Renilla luciferase may nonspecifically absorb to RSV particles, or firefly luciferase may be incorporated efficiently into budding RSV virions. Either scenario would render the protein inaccessible to purification strategies designed to preserve the infectivity of the virus stock.

A variety of different approaches were developed to control protein steady state levels *in cellulo*. However, only the very recently pioneered SMASh technology operates as a single-chain system and returns the stabilized protein in its near-native state.[39] Repeated passaging of the RSV recombinant harboring a fireSMASh open reading frame furthermore confirmed that the tag is genetically stable in the RSV background. These features make the technology uniquely suitable for applications in recombinant virions and allow, for instance, a controlled shut-off of virus replication *in vitro* and *in vivo*.[39] Applied to reporter viruses for HTS, SMASh provides an effective strategy for removing purification-resistant reporter proteins from virus stocks.

Test screening of the LOPAC1208 library in 384-well format using the fully validated assay correctly identified licensed antiviral therapeutics present in the library. In addition, Gemcitabine reportedly has antiretroviral and anti-influenza virus activity,[49,50] and compound blocking purine or pyrimidine biosynthesis was recognized in several previous drug screens as broad-spectrum antivirals.[30,58,59] Taken together, the hits in groups (i) and (ii) that emerged from our assay are therefore fully consistent with known antiviral profiles, generating confidence in the accuracy of hit discovery by the protocol.

Of the other confirmed hits, Fenretinide and BNTX-7 selectively blocked RSV in our assay. Fenretinide is a synthetic retinoid derivative that was developed with anticancer and anti-cystic fibrosis end points.[60] The compound also suppresses HIV infection, which was originally attributed to enhanced viral endocytosis.[61] However, a recent study demonstrating strong anti-Dengue virus activity suggested upregulation of the host cell unfolded protein response pathway as an alternative mechanism of activity.[62] BNTX-7 is a selective opioid delta receptor antagonist.[63] Highly differential activity against RSV and IAV in our dose−response counterscreens excludes high cytotoxicity as the underlying cause of RSV inhibition, and comparable potency against both RSV A2-L19F-renilla and RSV A2-$L19F_{D489E}$-fireSMASh with distinct reporter technology argues against reporter interference. Opioid receptors are present on epithelial cells of the oral/respiratory tract.[64] Remarkably, altered opioid receptor signaling was found to correlate with disease severity in human RSV infection and a mouse model,[65] underscoring that a mechanistic evaluation of the role of opioid receptor signaling in RSV replication may uncover novel druggable targets. An assessment of the broader paramyxovirus indication spectrum of Fenretinide and BNTX-7 and a characterization of the underlying mechanism for selective RSV inhibition are currently underway.

PMEG hydrate blocked both IAV and RSV reporter strains. The compound is an acyclic nucleotide analogue that results in DNA chain termination after conversion to the active diphosphate PMEGpp and incorporation.[66] Prodrugs of PMEG such as GS-9191 are developed for the topical treatment of human papillomavirus infection.[67] A second prodrug analogue, GS-9219, acts antineoplastic in dogs with non-Hodgkin's lymphoma,[68] but an unacceptable safety profile halted a human trial.

Whereas the dual-pathogen approach inherently reduces the frequency of undesirable compounds from the pool of virus-specific hits, broad-spectrum candidates must be expected to include a substantial portion of cytotoxic or promiscuous entries.[32] In our test screen, more than half of the hit candidates blocking both reporter strains revealed cytotoxicity exceeding our cutoff value for follow-up counterscreens, highlighting the fact that a wide antiviral indication spectrum is often penalized by being linked to acute or chronic cytotoxicity.

Of the reporter virus-specific hits, compounds may be acting through reporter interference or, in the case of recRSV A2-$L19F_{D489E}$-fireSMASh, inhibition of the HCV-derived NS3 protease. Traditional virus yield-based secondary screens are suitable for addressing assay interference and NS3 protease blockage but are labor- and resource-intensive. Having generated a diverse panel of myxovirus reporter strains harboring distinct luciferases,[32] we demonstrate the feasibility of a rapid automated counterscreening strategy that examines hit candidate activity against a luciferase reporter with distinct substrate chemistry. In the case of recRSV A2-$L19F_{D489E}$-fireSMASh, this approach also addresses any NS3 protease liability, because the fireSMASh was replaced by recRSV A2-$L19F_{D489E}$-renilla. We predict that the newly developed technologies and screening strategies reported here can be applied to a range of clinically relevant viral targets and will prove to be effective in rapidly focusing developmental efforts on viable hit candidates.

■ ASSOCIATED CONTENT

Supporting Information

The Supporting Information is available free of charge on the ACS Publications website at DOI: 10.1021/acs.biochem.5b00623.

PubChem identifiers and chemical structures of the hit candidates listed in Table 2 (Table S1) (PDF)

DOI: 10.1021/acs.biochem.5b00623
Biochemistry 2015, 54, 5589−5604

AUTHOR INFORMATION

Corresponding Author

*Institute for Biomedical Sciences, Petit Science Center, Suite 712, Georgia State University, 100 Piedmont Ave., Atlanta, GA 30303-3222. E-mail: rplemper@gsu.edu. Phone: 404-413-3579.

Funding

This work was supported, in part, by Public Health Service Grants AI071002, AI119196, and HD079327 from the National Institute of Allergy and Infectious Diseases and The Eunice Kennedy Shriver National Institute of Child Health and Human Development (to R.K.P.).

Notes

The authors declare the following competing financial interest(s): R.K.P. and D.Y. are inventors of a pending patent application concerning reporter virus technology described in this study.

ACKNOWLEDGMENTS

We are grateful to D. Steinhauer for kindly providing the IAV-WSN rescue system, R. Cox for help with computer artwork, Y. Hu for technical assistance, R. T. Jacob for IT assistance, M. Ndungu and M. T. Saindane for chemical synthesis, M. L. Moore for providing the RSV reverse genetics system, and A. L. Hammond for critical reading of the manuscript. The MScreen software package was kindly provided by the Center for Chemical Genomics of the University of Michigan under a license agreement by the University of Michigan Office of Technology Transfer. JChem was used for structure database management, search, and prediction [JChem 6.2, 2014, ChemAxon (http://www.chemaxon.com)]. Marvin was employed for drawing, displaying, and characterizing chemical structures, substructures, and reactions [Marvin 14.9.22.0, 2014, ChemAxon (http://www.chemaxon.com)].

REFERENCES

(1) Stiver, G. (2003) The treatment of influenza with antiviral drugs. *Cmaj 168*, 49−56.

(2) Thompson, W. W., Shay, D. K., Weintraub, E., Brammer, L., Cox, N., Anderson, L. J., and Fukuda, K. (2003) Mortality associated with influenza and respiratory syncytial virus in the United States. *JAMA 289*, 179−186.

(3) Hall, C. B. (2001) Respiratory syncytial virus and parainfluenza virus. *N. Engl. J. Med. 344*, 1917−1928.

(4) Mahadevia, P. J., Masaquel, A. S., Polak, M. J., and Weiner, L. B. (2012) Cost utility of palivizumab prophylaxis among pre-term infants in the United States: a national policy perspective. *J. Med. Econ 15*, 987−996.

(5) Collins, P. L., and Crowe, J. E., Jr. (2007) Respiratory Syncytial Virus and Metapneumoviruses. In *Fields Virology* (Knipe, D. M., and Howley, P. M., Eds.) 5the ed., pp 1601−1645, Lippincott, Williams, & Wilkins, Philadelphia.

(6) Elliot, A. J., and Fleming, D. M. (2008) Influenza and respiratory syncytial virus in the elderly. *Expert Rev. Vaccines 7*, 249−258.

(7) de Vries, R. D., Mesman, A. W., Geijtenbeek, T. B., Duprex, W. P., and de Swart, R. L. (2012) The pathogenesis of measles. *Curr. Opin. Virol. 2*, 248−255.

(8) Plemper, R. K., and Hammond, A. L. (2014) Synergizing vaccinations with therapeutics for measles eradication. *Expert Opin. Drug Discovery 9*, 201−214.

(9) DeVincenzo, J. P., El Saleeby, C. M., and Bush, A. J. (2005) Respiratory syncytial virus load predicts disease severity in previously healthy infants. *J. Infect. Dis. 191*, 1861−1868.

(10) El Saleeby, C. M., Bush, A. J., Harrison, L. M., Aitken, J. A., and Devincenzo, J. P. (2011) Respiratory syncytial virus load, viral dynamics, and disease severity in previously healthy naturally infected children. *J. Infect. Dis. 204*, 996−1002.

(11) Weiner, L. B., Masaquel, A. S., Polak, M. J., and Mahadevia, P. J. (2012) Cost-effectiveness analysis of palivizumab among pre-term infant populations covered by Medicaid in the United States. *J. Med. Econ 15*, 997−1018.

(12) Hall, C. B., Granoff, D. M., Gromisch, D. S., Halsey, N. A., Kohl, S., Marcuse, E. K., Marks, M. I., Nankervis, G. A., Pickering, L. K., Scott, G. B., Steele, R. W., Yogev, R., Peter, G., Bart, K. J., Broome, C., Hardegree, M. C., Jacobs, R. F., Macdonald, N. E., Orenstein, W. A., and Rabinovich, G. (1993) Use of Ribavirin in the Treatment of Respiratory Syncytial Virus-Infection. *Pediatrics 92*, 501−504.

(13) Beigel, J., and Bray, M. (2008) Current and future antiviral therapy of severe seasonal and avian influenza. *Antiviral Res. 78*, 91−102.

(14) Gatherer, D. (2009) The 2009 H1N1 influenza outbreak in its historical context. *J. Clin. Virol. 45*, 174−178.

(15) Li, Q., Zhou, L., Zhou, M., Chen, Z., Li, F., Wu, H., Xiang, N., Chen, E., Tang, F., Wang, D., Meng, L., Hong, Z., Tu, W., Cao, Y., Li, L., Ding, F., Liu, B., Wang, M., Xie, R., Gao, R., Li, X., Bai, T., Zou, S., He, J., Hu, J., Xu, Y., Chai, C., Wang, S., Gao, Y., Jin, L., Zhang, Y., Luo, H., Yu, H., He, J., Li, Q., Wang, X., Gao, L., Pang, X., Liu, G., Yan, Y., Yuan, H., Shu, Y., Yang, W., Wang, Y., Wu, F., Uyeki, T. M., and Feng, Z. (2014) Epidemiology of human infections with avian influenza A(H7N9) virus in China. *N. Engl. J. Med. 370*, 520−532.

(16) Taubenberger, J. K., and Morens, D. M. (2006) 1918 Influenza: the mother of all pandemics. *Emerging Infect. Dis. 12*, 15−22.

(17) Okomo-Adhiambo, M., Nguyen, H. T., Abd Elal, A., Sleeman, K., Fry, A. M., and Gubareva, L. V. (2014) Drug susceptibility surveillance of influenza viruses circulating in the United States in 2011−2012: application of the WHO antiviral working group criteria. *Influenza Other Respir. Viruses 8*, 258−265.

(18) Marjuki, H., Mishin, V. P., Chesnokov, A. P., Jones, J., De La Cruz, J. A., Sleeman, K., Tamura, D., Nguyen, H. T., Wu, H. S., Chang, F. Y., Liu, M. T., Fry, A. M., Cox, N. J., Villanueva, J. M., Davis, C. T., and Gubareva, L. V. (2015) Characterization of Drug-Resistant Influenza A(H7N9) Variants Isolated From an Oseltamivir-Treated Patient in Taiwan. *J. Infect. Dis. 211*, 249.

(19) McKimm-Breschkin, J. L. (2013) Influenza neuraminidase inhibitors: antiviral action and mechanisms of resistance. *Influenza Other Respir. Viruses 7* (Suppl. 1), 25−36.

(20) Fiore, A. E., Fry, A., Shay, D., Gubareva, L., Bresee, J. S., Uyeki, T. M., and Centers for Disease, C., and Prevention (2011) Antiviral agents for the treatment and chemoprophylaxis of influenza — recommendations of the Advisory Committee on Immunization Practices (ACIP). *MMWR Recomm Rep 60*, 1−24.

(21) Jefferson, T., Jones, M. A., Doshi, P., Del Mar, C. B., Heneghan, C. J., Hama, R., and Thompson, M. J. (2012) Neuraminidase inhibitors for preventing and treating influenza in healthy adults and children. *Cochrane Database Syst. Rev. 1*, CD008965.

(22) Torjesen, I. (2014) Cochrane review questions effectiveness of neuraminidase inhibitors. *BMJ. 348*, g2675.

(23) Jefferson, T., and Doshi, P. (2014) Multisystem failure: the story of anti-influenza drugs. *BMJ. 348*, g2263.

(24) Doshi, P., and Jefferson, T. (2014) Clinical trials: Tamiflu reviewers respond to critics. *Nature 509*, 288.

(25) Johnson, D. (2009) Croup. *Clin Evid (Online)*, Vol. *2009*.

(26) Bjornson, C. L., and Johnson, D. W. (2008) Croup. *Lancet 371*, 329−339.

(27) Salerno, D., Hasham, M. G., Marshall, R., Garriga, J., Tsygankov, A. Y., and Grana, X. (2007) Direct inhibition of CDK9 blocks HIV-1 replication without preventing T-cell activation in primary human peripheral blood lymphocytes. *Gene 405*, 65−78.

(28) Schang, L. M. (2006) First demonstration of the effectiveness of inhibitors of cellular protein kinases in antiviral therapy. *Expert Rev. Anti-Infect. Ther. 4*, 953−956.

(29) Prussia, A., Thepchatri, P., Snyder, J. P., and Plemper, R. K. (2011) Systematic Approaches towards the Development of Host-Directed Antiviral Therapeutics. *Int. J. Mol. Sci. 12*, 4027−4052.

DOI: 10.1021/acs.biochem.5b00623
Biochemistry 2015, 54, 5589−5604

(30) Krumm, S. A., Ndungu, J. M., Yoon, J. J., Dochow, M., Sun, A., Natchus, M., Snyder, J. P., and Plemper, R. K. (2011) Potent host-directed small-molecule inhibitors of myxovirus RNA-dependent RNA-polymerases. *PLoS One 6*, e20069.
(31) Schwegmann, A., and Brombacher, F. (2008) Host-directed drug targeting of factors hijacked by pathogens. *Sci. Signaling 1*, re8.
(32) Yan, D., Krumm, S. A., Sun, A., Steinhauer, D. A., Luo, M., Moore, M. L., and Plemper, R. K. (2013) Dual myxovirus screen identifies a small-molecule agonist of the host antiviral response. *J. Virol 87*, 11076−11087.
(33) Buchholz, U. J., Finke, S., and Conzelmann, K. K. (1999) Generation of bovine respiratory syncytial virus (BRSV) from cDNA: BRSV NS2 is not essential for virus replication in tissue culture, and the human RSV leader region acts as a functional BRSV genome promoter. *J. Virol 73*, 251−259.
(34) Hoffmann, E., Neumann, G., Kawaoka, Y., Hobom, G., and Webster, R. G. (2000) A DNA transfection system for generation of influenza A virus from eight plasmids. *Proc. Natl. Acad. Sci. U. S. A. 97*, 6108−6113.
(35) Heaton, N. S., Leyva-Grado, V. H., Tan, G. S., Eggink, D., Hai, R., and Palese, P. (2013) In vivo bioluminescent imaging of influenza a virus infection and characterization of novel cross-protective monoclonal antibodies. *J. Virol 87*, 8272−8281.
(36) Manicassamy, B., Manicassamy, S., Belicha-Villanueva, A., Pisanelli, G., Pulendran, B., and Garcia-Sastre, A. (2010) Analysis of in vivo dynamics of influenza virus infection in mice using a GFP reporter virus. *Proc. Natl. Acad. Sci. U. S. A. 107*, 11531−11536.
(37) Donnelly, M. L., Hughes, L. E., Luke, G., Mendoza, H., ten Dam, E., Gani, D., and Ryan, M. D. (2001) The 'cleavage' activities of foot-and-mouth disease virus 2A site-directed mutants and naturally occurring '2A-like' sequences. *J. Gen. Virol. 82*, 1027−1041.
(38) Hotard, A. L., Shaikh, F. Y., Lee, S., Yan, D., Teng, M. N., Plemper, R. K., Crowe, J. E., Jr., and Moore, M. L. (2012) A stabilized respiratory syncytial virus reverse genetics system amenable to recombination-mediated mutagenesis. *Virology 434*, 129−136.
(39) Chung, H. K., Jacobs, C. L., Huo, Y., Yang, J., Krumm, S. A., Plemper, R. K., Tsien, R. Y., and Lin, M. Z. (2015) Tunable and reversible drug control of protein production via a self-excising degron. *Nat. Chem. Biol. 11*, 713.
(40) Jacob, R. T., Larsen, M. J., Larsen, S. D., Kirchhoff, P. D., Sherman, D. H., and Neubig, R. R. (2012) MScreen: an integrated compound management and high-throughput screening data storage and analysis system. *J. Biomol. Screening 17*, 1080−1087.
(41) Zhang, J. H., Chung, T. D., and Oldenburg, K. R. (1999) A Simple Statistical Parameter for Use in Evaluation and Validation of High Throughput Screening Assays. *J. Biomol. Screening 4*, 67−73.
(42) Boutros, M., Bras, L. P., and Huber, W. (2006) Analysis of cell-based RNAi screens. *Genome Biol. 7*, R66.
(43) Tran, V., Moser, L. A., Poole, D. S., and Mehle, A. (2013) Highly sensitive real-time in vivo imaging of an influenza reporter virus reveals dynamics of replication and spread. *J. Virol 87*, 13321−13329.
(44) Lazarowitz, S. G., Goldberg, A. R., and Choppin, P. W. (1973) Proteolytic cleavage by plasmin of the HA polypeptide of influenza virus: host cell activation of serum plasminogen. *Virology 56*, 172−180.
(45) Yan, D., Lee, S., Thakkar, V. D., Luo, M., Moore, M. L., and Plemper, R. K. (2014) Cross-resistance mechanism of respiratory syncytial virus against structurally diverse entry inhibitors. *Proc. Natl. Acad. Sci. U. S. A. 111*, E3441−3449.
(46) Scola, P. M., Sun, L. Q., Wang, A. X., Chen, J., Sin, N., Venables, B. L., Sit, S. Y., Chen, Y., Cocuzza, A., Bilder, D. M., D'Andrea, S. V., Zheng, B., Hewawasam, P., Tu, Y., Friborg, J., Falk, P., Hernandez, D., Levine, S., Chen, C., Yu, F., Sheaffer, A. K., Zhai, G., Barry, D., Knipe, J. O., Han, Y. H., Schartman, R., Donoso, M., Mosure, K., Sinz, M. W., Zvyaga, T., Good, A. C., Rajamani, R., Kish, K., Tredup, J., Klei, H. E., Gao, Q., Mueller, L., Colonno, R. J., Grasela, D. M., Adams, S. P., Loy, J., Levesque, P. C., Sun, H., Shi, H., Sun, L., Warner, W., Li, D., Zhu, J., Meanwell, N. A., and McPhee, F. (2014) The discovery of asunaprevir (BMS-650032), an orally efficacious NS3 protease inhibitor for the treatment of hepatitis C virus infection. *J. Med. Chem. 57*, 1730−1752.
(47) Zhang, J. H., Chung, T. D. Y., and Oldenburg, K. R. (1999) A simple statistical parameter for used in evaluation and validation of high throughput screening assays. *J. Biomol. Screening 4*, 67−73.
(48) Cianci, C., Yu, K. L., Combrink, K., Sin, N., Pearce, B., Wang, A., Civiello, R., Voss, S., Luo, G., Kadow, K., Genovesi, E. V., Venables, B., Gulgeze, H., Trehan, A., James, J., Lamb, L., Medina, I., Roach, J., Yang, Z., Zadjura, L., Colonno, R., Clark, J., Meanwell, N., and Krystal, M. (2004) Orally active fusion inhibitor of respiratory syncytial virus. *Antimicrob. Agents Chemother. 48*, 413−422.
(49) Denisova, O. V., Kakkola, L., Feng, L., Stenman, J., Nagaraj, A., Lampe, J., Yadav, B., Aittokallio, T., Kaukinen, P., Ahola, T., Kuivanen, S., Vapalahti, O., Kantele, A., Tynell, J., Julkunen, I., Kallio-Kokko, H., Paavilainen, H., Hukkanen, V., Elliott, R. M., De Brabander, J. K., Saelens, X., and Kainov, D. E. (2012) Obatoclax, saliphenylhalamide, and gemcitabine inhibit influenza a virus infection. *J. Biol. Chem. 287*, 35324−35332.
(50) Clouser, C. L., Holtz, C. M., Mullett, M., Crankshaw, D. L., Briggs, J. E., O'Sullivan, M. G., Patterson, S. E., and Mansky, L. M. (2012) Activity of a novel combined antiretroviral therapy of gemcitabine and decitabine in a mouse model for HIV-1. *Antimicrob. Agents Chemother. 56*, 1942−1948.
(51) Arteaga, C. L., Brown, T. D., Kuhn, J. G., Shen, H. S., O'Rourke, T. J., Beougher, K., Brentzel, H. J., Von Hoff, D. D., and Weiss, G. R. (1989) Phase I clinical and pharmacokinetic trial of Brequinar sodium (DuP 785; NSC 368390). *Cancer Res. 49*, 4648−4653.
(52) Nichol, C. A., and Welch, A. D. (1950) On the mechanism of action of aminopterin. *Exp. Biol. Med. 74*, 403−411.
(53) Beyleveld, G., White, K. M., Ayllon, J., and Shaw, M. L. (2013) New-generation screening assays for the detection of anti-influenza compounds targeting viral and host functions. *Antiviral Res. 100*, 120−132.
(54) DeVincenzo, J. P., Whitley, R. J., Mackman, R. L., Scaglioni-Weinlich, C., Harrison, L., Farrell, E., McBride, S., Lambkin-Williams, R., Jordan, R., Xin, Y., Ramanathan, S., O'Riordan, T., Lewis, S. A., Li, X., Toback, S. L., Lin, S. L., and Chien, J. W. (2014) Oral GS-5806 activity in a respiratory syncytial virus challenge study. *N. Engl. J. Med. 371*, 711−722.
(55) Samuel, D., Xing, W., Niedziela-Majka, A., Wong, J., Brendza, K., Jordan, R., Perron, M., Sperandio, D., Liu, X., Sakowicz, R., and Mackman, R. (2014) V-1814. GS-5806 Inhibits Pre- to Post-fusion Conformational Changes of the RSV Fusion Protein. Interscience Conference of Antimicrobial Agents and Chemotherapy (ICAAC). September 5−9, 2014; Washington, DC.
(56) Weisshaar, M., Cox, R., and Plemper, R. K. (2015) Blocking Respiratory Syncytial Virus Entry: A Story with Twists. *DNA Cell Biol. 34*, 505.
(57) Hallak, L. K., Spillmann, D., Collins, P. L., and Peeples, M. E. (2000) Glycosaminoglycan sulfation requirements for respiratory syncytial virus infection. *J. Virol 74*, 10508−10513.
(58) Shanley, J. D., and Debs, R. J. (1989) The folate antagonist, methotrexate, is a potent inhibitor of murine and human cytomegalovirus in vitro. *Antiviral Res. 11*, 99−106.
(59) Hoffmann, H. H., Kunz, A., Simon, V. A., Palese, P., and Shaw, M. L. (2011) Broad-spectrum antiviral that interferes with de novo pyrimidine biosynthesis. *Proc. Natl. Acad. Sci. U. S. A. 108*, 5777−5782.
(60) Guilbault, C., De Sanctis, J. B., Wojewodka, G., Saeed, Z., Lachance, C., Skinner, T. A., Vilela, R. M., Kubow, S., Lands, L. C., Hajduch, M., Matouk, E., and Radzioch, D. (2008) Fenretinide corrects newly found ceramide deficiency in cystic fibrosis. *Am. J. Respir. Cell Mol. Biol. 38*, 47−56.
(61) Finnegan, C. M., and Blumenthal, R. (2006) Fenretinide inhibits HIV infection by promoting viral endocytosis. *Antiviral Res. 69*, 116−123.
(62) Fraser, J. E., Rawlinson, S. M., Wang, C., Jans, D. A., and Wagstaff, K. M. (2014) Investigating dengue virus nonstructural protein 5 (NS5) nuclear import. *Methods Mol. Biol. 1138*, 301−328.
(63) Beaudry, H., Gendron, L., and Moron, J. A. (2015) Implication of delta opioid receptor subtype 2 but not delta opioid receptor

DOI: 10.1021/acs.biochem.5b00623
Biochemistry 2015, 54, 5589−5604

subtype 1 in the development of morphine analgesic tolerance in a rat model of chronic inflammatory pain. *Eur. J. Neurosci 41*, 901−907.
(64) Charbaji, N., Schafer-Korting, M., and Kuchler, S. (2012) Morphine stimulates cell migration of oral epithelial cells by delta-opioid receptor activation. *PLoS One 7*, e42616.
(65) Salimi, V., Hennus, M. P., Mokhtari-Azad, T., Shokri, F., Janssen, R., Hodemaekers, H. M., Rygiel, T. P., Coenjaerts, F. E., Meyaard, L., and Bont, L. (2013) Opioid receptors control viral replication in the airways. *Crit. Care Med. 41*, 205−214.
(66) Tsai, C. Y., Ray, A. S., Tumas, D. B., Keating, M. J., Reiser, H., and Plunkett, W. (2009) Targeting DNA repair in chronic lymphocytic leukemia cells with a novel acyclic nucleotide analogue, GS-9219. *Clin. Cancer Res. 15*, 3760−3769.
(67) Wolfgang, G. H., Shibata, R., Wang, J., Ray, A. S., Wu, S., Doerrfler, E., Reiser, H., Lee, W. A., Birkus, G., Christensen, N. D., Andrei, G., and Snoeck, R. (2009) GS-9191 is a novel topical prodrug of the nucleotide analog 9-(2-phosphonylmethoxyethyl)guanine with antiproliferative activity and possible utility in the treatment of human papillomavirus lesions. *Antimicrob. Agents Chemother. 53*, 2777−2784.
(68) Vail, D. M., Thamm, D. H., Reiser, H., Ray, A. S., Wolfgang, G. H., Watkins, W. J., Babusis, D., Henne, I. N., Hawkins, M. J., Kurzman, I. D., Jeraj, R., Vanderhoek, M., Plaza, S., Anderson, C., Wessel, M. A., Robat, C., Lawrence, J., and Tumas, D. B. (2009) Assessment of GS-9219 in a pet dog model of non-Hodgkin's lymphoma. *Clin. Cancer Res. 15*, 3503−3510.
(69) Zhang, J., Stevens, M. F., and Bradshaw, T. D. (2012) Temozolomide: mechanisms of action, repair and resistance. *Curr. Mol. Pharmacol 5*, 102−114.
(70) Gribaudo, G., Riera, L., Lembo, D., De Andrea, M., Johnson, L. F., and Landolfo, S. (2001) The anticytomegaloviral activity of raltitrexed is abrogated in quiescent mouse fibroblasts that overexpress thymidylate synthase. *Virus Res. 73*, 57−65.
(71) Guerrero, C. A., Murillo, A., and Acosta, O. (2012) Inhibition of rotavirus infection in cultured cells by N-acetyl-cysteine, PPARgamma agonists and NSAIDs. *Antiviral Res. 96*, 1−12.
(72) Morlet, N., Stayt, J., Vaegan, Salonikas, C., Naidoo, D., Crouch, R., Graham, G., and Coroneo, M. (1999) Etoposide as a virocidal anticytomegalovirus therapy: intravitreal toxicology and pharmacology in rabbits. *Aust N Z. J. Ophthalmol 27*, 342−349.
(73) Mohammadgholi, A., Rabbani-Chadegani, A., and Fallah, S. (2013) Mechanism of the interaction of plant alkaloid vincristine with DNA and chromatin: spectroscopic study. *DNA Cell Biol. 32*, 228−235.
(74) Loh, P. C., and Soergel, M. (1965) Growth characteristics of reovirus type 2: actinomycin D and the synthesis of viral RNA. *Proc. Natl. Acad. Sci. U. S. A. 54*, 857−863.
(75) Wan, Z., and Chen, X. (2014) Triptolide inhibits human immunodeficiency virus type 1 replication by promoting proteasomal degradation of Tat protein. *Retrovirology 11*, 88.
(76) Cova, L., Trepo, C., Narayan, R., Borowski, P., Kulikowski, T., and Zagorski-Ostoja, W. (2006) Epirubicine hydrochloride for treating hepatitis C virus. EP register EP1721614 A1.
(77) Cao, J., Forrest, J. C., and Zhang, X. (2015) A screen of the NIH Clinical Collection small molecule library identifies potential anti-coronavirus drugs. *Antiviral Res. 114*, 1−10.
(78) Patel, D. A., Patel, A. C., Nolan, W. C., Zhang, Y., and Holtzman, M. J. (2012) High throughput screening for small molecule enhancers of the interferon signaling pathway to drive next-generation antiviral drug discovery. *PLoS One 7*, e36594.
(79) Fischer, M. A., Smith, J. L., Shum, D., Stein, D. A., Parkins, C., Bhinder, B., Radu, C., Hirsch, A. J., Djaballah, H., Nelson, J. A., and Fruh, K. (2013) Flaviviruses are sensitive to inhibition of thymidine synthesis pathways. *Journal of virology 87*, 9411−9419.
(80) Sidwell, R. W., Arnett, G., and Schabel, F. M., Jr. (1972) In vitro effect of a variety of biologically active compounds on human cytomegalovirus. *Chemotherapy 17*, 259−282.
(81) Yeo, K. L., Chen, Y. L., Xu, H. Y., Dong, H., Wang, Q. Y., Yokokawa, F., and Shi, P. Y. (2015) Synergistic suppression of dengue virus replication using a combination of nucleoside analogs and nucleoside synthesis inhibitors. *Antimicrob. Agents Chemother. 59*, 2086−2093.
(82) Lucas-Hourani, M., Dauzonne, D., Jorda, P., Cousin, G., Lupan, A., Helynck, O., Caignard, G., Janvier, G., Andre-Leroux, G., Khiar, S., Escriou, N., Despres, P., Jacob, Y., Munier-Lehmann, H., Tangy, F., and Vidalain, P. O. (2013) Inhibition of pyrimidine biosynthesis pathway suppresses viral growth through innate immunity. *PLoS Pathog. 9*, e1003678.
(83) Demicheli, V., Jefferson, T., Rivetti, D., and Deeks, J. (2000) Prevention and early treatment of influenza in healthy adults. *Vaccine 18*, 957−1030.
(84) Smee, D. F., Bray, M., and Huggins, J. W. (2001) Antiviral activity and mode of action studies of ribavirin and mycophenolic acid against orthopoxviruses in vitro. *Antiviral Chem. Chemother. 12*, 327−335.
(85) Fox, T., Coll, J. T., Xie, X., Ford, P. J., Germann, U. A., Porter, M. D., Pazhanisamy, S., Fleming, M. A., Galullo, V., Su, M. S., and Wilson, K. P. (1998) A single amino acid substitution makes ERK2 susceptible to pyridinyl imidazole inhibitors of p38 MAP kinase. *Protein Sci. 7*, 2249−2255.
(86) Matharu, D. S., Flaherty, D. P., Simpson, D. S., Schroeder, C. E., Chung, D., Yan, D., Noah, J. W., Jonsson, C. B., White, E. L., Aube, J., Plemper, R. K., Severson, W. E., and Golden, J. E. (2014) Optimization of potent and selective quinazolinediones: inhibitors of respiratory syncytial virus that block RNA-dependent RNA-polymerase complex activity. *J. Med. Chem. 57*, 10314−10328.
(87) Yan, D., Lee, S., Thakkar, V. D., Luo, M., Moore, M. L., and Plemper, R. K. (2014) Cross-resistance mechanism of respiratory syncytial virus against structurally diverse entry inhibitors. *Proc. Natl. Acad. Sci. U.S.A. 111*, E3441−E3449.
(88) Krumm, S. A., Yan, D., Hovingh, E. S., Evers, T. J., Enkirch, T., Reddy, G. P., Sun, A., Saindane, M. T., Arrendale, R. F., Painter, G., Liotta, D. C., Natchus, M. G., von Messling, V., and Plemper, R. K. (2014) An orally available, small-molecule polymerase inhibitor shows efficacy against a lethal morbillivirus infection in a large animal model. *Sci. Transl. Med. 6*, 232ra252.
(89) Yoon, J. J., Krumm, S. A., Ndungu, J. M., Hoffman, V., Bankamp, B., Rota, P. A., Sun, A., Snyder, J. P., and Plemper, R. K. (2009) Target analysis of the experimental measles therapeutic AS-136A. *Antimicrob. Agents Chemother. 53*, 3860−3870.

DOI: 10.1021/acs.biochem.5b00623
Biochemistry 2015, 54, 5589−5604